KONA Powder and Particle Journal

KONA Powder and Particle Journal No. 43 (2026) 155–173/https://doi.org/10.14356/kona.2026008 Review Paper

High Thermal Conductivity of Silicon Nitride Ceramics: A Review †

Yusen Duan [1]*, Yanyu Ye [1,2], Ning Liu [3], Wenyu Tang [1], Hu Ruan [1] and Jingxian Zhang [1]*

[1] *State Key Laboratory of High Performance Ceramics and Superfine Microstructures, Shanghai Institute of Ceramics, Chinese Academy of Sciences, China*

[2] *University of Chinese Academy of Sciences, China*

[3] *Engineering & Technology Center for Aerospace Materials, Wuzhen Laboratory, China*

Silicon-nitride ceramic substrates exhibit high thermal conductivity, high electrical insulation, high mechanical strength, low expansion. The Cu-clad ceramic substrate is the key material for the encapsulation of insulated gate bipolar transistor modules. In this review, we divide the research of high thermal conductivity silicon nitride ceramics into four stages: 1) exploration of thermal conductivity with different sintering additives; 2) using the anisotropy of silicon nitride grains to improve the thermal conductivity, through the addition of silicon nitride grain seeds combined with tape casting technology, sintered to obtain a thermal conductivity of 155 W/(m·K) silicon nitride, and with the development of the strong magnetic field alignment technology in the later stage, the thermal conductivity can be increased to 176 W/(m·K); 3) using sintered of reaction-bonded silicon nitride technology to improve thermal conductivity, thermal conductivity can be increased to about 180 W/(m·K); 4) the application of high thermal conductivity silicon nitride ceramic substrate. Finally, future preparation methods and applications of high thermal conductivity silicon nitride ceramics are envisioned.

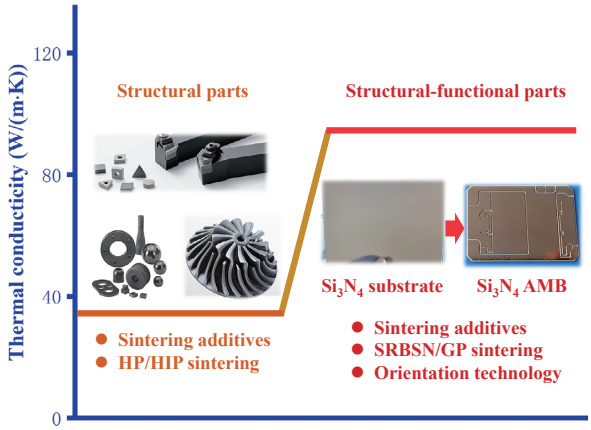

Keywords: silicon nitride, thermal conductivity, microstructure, non-oxide sintering additives, lattice defects

1. Introduction

With third-generation semiconductors, SiC, GaN, etc., gradually replacing traditional Si semiconductors, the power electronics industry, aerospace, automotive, and other fields in the application of electronic energy devices are faced with the challenge of high current and high-power density (Okumura, 2006). For example, the insulated gate bipolar transistor (IGBT) structure shown in **Fig. 1** (Wang et al., 2014a) presents a cross-section of a conventional indirect liquid cooling system and a newly developed direct liquid cooling system. The new IGBT module has a copper base plate with pin fins, and coolant flows directly into the pin fin area. In conventional and new IGBT modules, the insulating substrate material is an indispensable part of the module design. With the continuous updating and modernization of the module design, the thickness of the required substrate material is also significantly reduced. Therefore, the ceramic substrate must be equipped with excellent mechanical and thermal conductivity. Al_2O_3 ceramics have poor thermal conductivity (20 W/(m·K)) (Tiwari and Feng, 2024). AlN ceramics have poor thermal shock resistance, fracture toughness, and other properties. The increase in the number of cycles is prone to microcracks at the interface, resulting in circuit detachment, thus seriously affecting the service life of the device. Therefore, traditional Al_2O_3 and AlN ceramic substrates have difficulty meeting the requirements for use (Zhao et al., 2024).

Silicon nitride (Si_3N_4) was discovered in the 19th century, and researchers first investigated the synthesis of Si_3N_4 powders using methods such as direct synthesis and carbothermal reduction (Moulson, 1979; Riley, 2000). Due to their excellent high-temperature mechanical properties, β-Si_3N_4 ceramics received widespread attention in the mid-20th century. As a typical structural ceramic material, Si_3N_4 ceramics have high flexural strength (up to 1.4 GPa), fracture toughness (up to 12.4 MPa·$m^{1/2}$) (Imamura et al., 2000), thermal shock resistance, good abrasion resistance, high Weibull modulus (20–50), high-temperature strength (70–80 % of the room-temperature strength at 1450 °C) (Krause Jr et al., 2001), and low thermal expansion coefficient (10^{-6} /K), which can be used as automotive engine

† Received 23 July 2024; Accepted 31 October 2024
J-STAGE Advance published online 25 April 2025

* Corresponding author: Yusen Duan; Jingxian Zhang
Add: Shanghai 200050, China
E-mail: duanyusen@mail.sic.ac.cn(Y.D.); jxzhang@mail.sic.ac.cn (J.Z.)
TEL: +86-021-5241-2165 FAX: +86-021-5241-2165

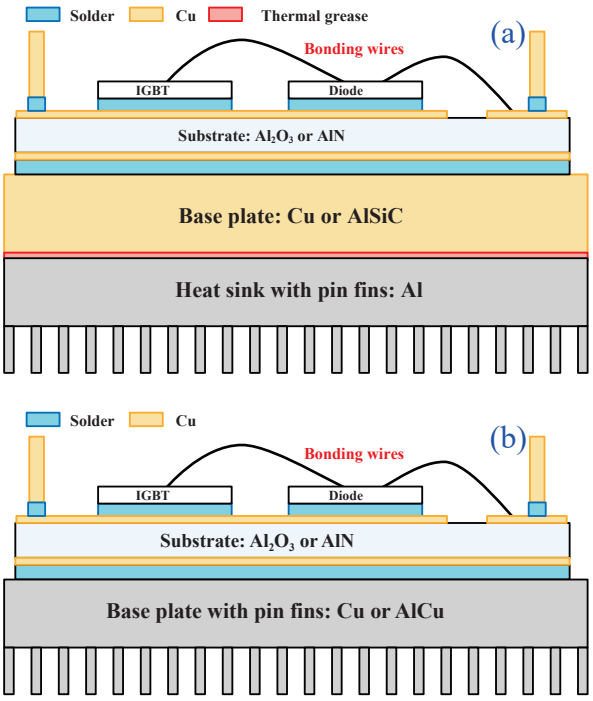

Fig. 1 Comparison of conventional IGBT module and new IGBT module. Adapted with permission from Ref. (Wang et al., 2014a). Copyright 2014, Elsevier.

parts, heat exchangers, pump seal parts, ball bearings, cutting tools, and ceramic armor (Ogata et al., 2004).

However, the thermal conductivity of Si_3N_4 ceramics is usually below 70 W/(m·K) (Matovic et al., 2004). If Si_3N_4 ceramics have both excellent thermal conductivity and mechanical properties, Si_3N_4 would undoubtedly be an attractive substrate material for high-power electronic device applications. In recent years, numerous researchers have been captivated by the prospect of enhancing thermal conductivity of Si_3N_4 ceramics using diverse methods. In this review, the crystal structure, material microstructural characteristics, and thermal conductivity research progress of Si_3N_4 ceramics are reviewed comprehensively. The main factors affecting the thermal conductivity of Si_3N_4 ceramics include lattice defects, grain-boundary film composition and thickness, purity and type of raw materials, grain size and distribution, sintering method, and sintering additive types and content.

2. The properties of Si_3N_4 ceramics

Si_3N_4 has two main crystal structures under ambient conditions, i.e., trigonal α-Si_3N_4 (space group: $P3_1/c$) and hexagonal β-Si_3N_4 (space group: $P6_3/m$). The crystal structure α-Si_3N_4 and β-Si_3N_4 are shown in **Fig. 2** (Legut et al., 2014). Both α and β phases are characterized by planar structures parallel to the basal plane. The Si–N layers in the β phase are stacked along the *c*-axis in an alternate sequence …ABABAB…, whereas in the α phase, the sequence becomes …ABCDABCD…, where the CD layers

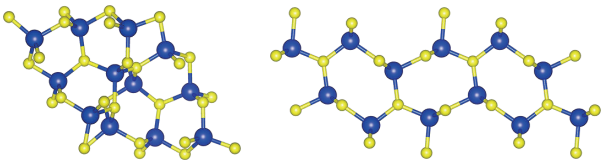

Fig. 2 Crystal structures of α-Si_3N_4 **(left)** and β-Si_3N_4 **(right)** viewed along the *c*-axis. The N and Si atoms are indicated by yellow and blue balls, respectively. (Original work by the authors.)

are related to the AB layers by a *c*-glide plane. Thus, the *c*-axis of the α phase (unit cell containing 28 atoms) is approximately twice that of the β phase (unit cell containing 14 atoms). In addition, the α phase can accommodate relatively large impurity ions because it contains interstices between the distorted layers. The lattice of α-Si_3N_4 can incorporate a variable amount of oxygen ions, which can exist both as a surface oxide-rich layer. The oxygen content (ranging from 0.90 % to 1.48 %) changes the composition of α-Si_3N_4 and thus affects the unit cell dimensions of this phase (Niihara and Hirai, 1977).

Due to the small sintering driving force, Si_3N_4 ceramics cannot be densified by solid-phase sintering (Tanaka et al., 1987). Therefore, sintering additives are necessary, which can change into liquid phases at high sintering temperatures. Through the dissolution-precipitation, dense Si_3N_4 ceramics are prepared with grain growth and pore diffusion (Abe, 1990). The type and content of the liquid phase significantly affect the performance of Si_3N_4 ceramics. The liquid phase formed by sintering aids in the high-temperature stage can be uniformly distributed among the ceramic particles by capillary forces, which promotes the sintering of Si_3N_4 ceramics. α-Si_3N_4 undergoes crystalline transformation and Ostwald ripening process (Kingery, 1959; Kingery and Narasimhan, 1959; Zhu and Sakka, 2008).

The researchers, by comparing the parameters of Si_3N_4 and SiC with respect to thermal conductivity (see **Table 1**), concluded that both intrinsic defects reduce the thermal conductivity of Si_3N_4 ceramics by reducing the mean free range of the phonons, and therefore the phonons have a larger range of freedom in larger sizes of β-Si_3N_4 crystals, and it was shown that when the number of atoms $n = 14$, the room-temperature intrinsic thermal conductivity of Si_3N_4 ceramics is about 200 W/(m·K), and the room-temperature intrinsic thermal conductivity of Si_3N_4 ceramics is about 320 W/(m·K) when the atomic number $n = 7$ (Haggerty and Lightfoot, 1995).

The main preparation methods are hot-pressure sintering (HPs), gas-pressure sintering (GPs), sintered reaction-bonded silicon nitride (SRBSN), and pressureless sintering (PLs). By adopting SRBSN and heat-treating the samples for 60 h at 1900 °C with nitrogen pressure (1 MPa), the thermal conductivity was increased to 177 W/(m·K). As reported by (Hirao et al., 2017), the sintered Si_3N_4 ceramic with the highest thermal conductivity—approximately

Table 1 Summary of parameters controlling the thermal conductivities of SiC and Si_3N_4 (Haggerty et al., 1989).

Parameters	SiC	Si_3N_4
Debye temperature (θ_D)	807 °C	867 °C
Intermediate temperature ($1/3\theta_D$)	87 °C	151 °C
Low temperature ($1/6\theta_D$)	–93 °C	–60 °C
Gruneisen constant (γ)	0.76	0.72
Atoms per primitive cell (n)	2	28
Average atomic volume (δ^3)(cm^3)	~1.04×10^{-23}	~1.04×10^{-23}
Average atomic mass (M)(g/mol)	20.05	20.00

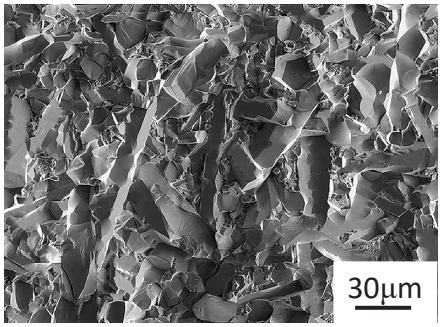

Fig. 3 Fractured surface of SRBSN with high thermal conductivity of 180 W/(m·K) and high fracture toughness of 11 MPa·$m^{1/2}$ (Hirao et al., 2017). Reprinted with permission from J-STAGE "open access".

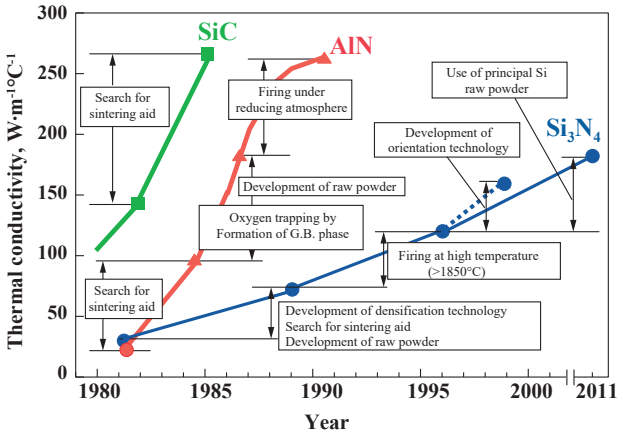

Fig. 4 Enhancement of thermal conductivity of Si_3N_4, AlN, and SiC ceramics (Watari, 2014). Reprinted with permission from J-STAGE "open access".

180 W/(m·K) using the same technique—exhibited the bending strength and fracture toughness of 600 MPa and 11 MPa·$m^{1/2}$, respectively (Zhou et al., 2011). **Fig. 3** shows that there is no obvious secondary phase between Si_3N_4 grains of high thermal conductivity Si_3N_4 ceramics, the size distribution of the grains is more uniform, and no abnormally grown grains are observed.

3. Research progress of Si_3N_4 ceramics about thermal conductivity

The evolution of Si_3N_4 ceramics' increased conductivity is shown in **Fig. 4** (Watari, 2014). There are basically several steps to the rise in thermal conductivity: 1) search for effective sintering aids for Si_3N_4 ceramics (including non-oxide sintering additives), development of high-purity fine powder, development of densification technology; 2) controlling sintering atmosphere and development of grain orientation; 3) selection of high-purity silicon powder raw materials. Meanwhile, throughout the research and development process, with the update of new equipment as well as sintering technology, the researchers also proposed some unique research ideas, including *in situ* lattice purification, strong magnetic field orientation, and hot-pressure flow sintering technology.

3.1 Effects of the sintering additives

Concerning optimization of Si_3N_4 raw material powders and selection of efficient sintering aids, the researchers developed a thermal decomposition method of imide for the preparation of high-purity and high-sintering-activity α-Si_3N_4 powders, which greatly lowered the sintering temperature and strongly improved the thermal conductivity of Si_3N_4 ceramics (Yamada, 1993). Researchers have also carried out a lot of work on the selection of sintering additives. For instance, Si_3N_4 ceramics prepared using MgO as an additive exhibited a thermal conductivity of 30 W/(m·K) (Tsukuma et al., 1981). Under the same conditions, hot-press sintered Si_3N_4 ceramics reached a maximum thermal diffusivity of 0.2 cm^2/s at 3 wt% MgO (Ziegler and Hasselman, 1981).

The thermal conductivities of Si_3N_4 ceramics obtained using Al_2O_3, Y_2O_3–Al_2O_3, Y_2O_3 as sintering additives are 16, 27 and 72 W/(m·K), respectively, indicating that Al_2O_3 has an important influence on the sintering temperature of α-Si_3N_4 powders, and that the sintering temperature of α-Si_3N_4 powders is greatly reduced, indicating that Al_2O_3 is unfavorable for thermal conductivity, while the use of Y_2O_3 is beneficial for obtaining high thermal conductivity (Watari et al., 1989).

As mentioned above, in 1995, Haggerty indicated that the room-temperature intrinsic thermal conductivity of

Si_3N_4 ceramics is approximately 320 W/(m·K). The researchers then combined high thermal conductivity silicon carbide and aluminum nitride ceramics with sintering technology to further optimize the thermal conductivity of Si_3N_4 ceramics. The thermal conductivity was enhanced to more than 100 W/(m·K) by increasing the sintering temperature and prolonging the holding time to promote the full growth and development of the grains in the liquid phase through the dissolution-precipitation process. For example, the Si_3N_4 ceramics with a thermal conductivity of 120 W/(m·K) were obtained by holding at 2000 °C for 4 h with Y_2O_3–Nd_2O_3 as sintering additives (Hirosaki et al., 1996). The thermal conductivity increased with the sintering temperature because of the decrease in the number of two-grain junctions due to grain growth. Considering the thermal conductivity of SiO_2-based glass, the thermal conductivity of the intergranular phases is much lower than that of Si_3N_4, ranging from 0.1 to 0.7 W/(m·K) (Ohashi et al., 1995). Thus, Si_3N_4. ceramics can be treated as a two-phase material composed of Si_3N_4 grains with high κ and intergranular phases with low κ. The thermal conductivity of two-phase materials depends on their individual thermal conductivity and the configuration of the two phases: parallel, dispersed, or serial.

Dense Si_3N_4 ceramics with high thermal conductivity were prepared by sintering α-Si_3N_4 powder compacts under gas pressure (1 MPa) at 1900 °C while utilizing only Yb_2O_3 as a sintering additive (Zhu et al., 2010b). The effects of Yb_2O_3 content, sample packing condition, and sintering time on the density, microstructure, and thermal conductivity were investigated. Plotting the density against the Yb_2O_3 content revealed a distinctive "N" shape, with almost full densification below and beyond the local minimum at 3 mol% Yb_2O_3. During sintering, the sample interacts with the reduced atmosphere and thus usually exhibits either a porous or dense outer surface layer, depending on the processing parameters. Once the phase transformation is completed, further densification is due to the combination of Ostwald ripening and coalescence via the solution–precipitation process. Moreover, the embedded condition did not affect the density when Yb_2O_3 addition was ⩾5 mol% but it significantly increased at <5 mol%. The embedded conditions allowed the samples with 1–2 mol% Yb_2O_3 to achieve relative densities of >95 % after 12 h of holding. The sintered sample under embedded conditions leads to more complete densification and a decrease in thermal conductivity from 119 to 94 W/(m·K) upon 1 mol% Yb_2O_3 addition.

Non-oxide sintering additives can effectively remove SiO_2 from the surface of α-Si_3N_4 powders. Si_3N_4 ceramics with a thermal conductivity of 140 W/(m·K) using Yb_2O_3–$MgSiN_2$ as a sintering additive were prepared (Hayashi et al., 2001b), and the specimen was sintered at 1950 °C for 48 h, while the thermal conductivity of the sample with Yb_2O_3–MgO added as an additive was only 122 W/(m·K) under the same sintering conditions. Then, a large number of literature reports focused on the optimization of sintering additives, including the selection of compounds with free oxygen content, like $MgSiN_2$, MgF_2, and YF_3. For instance, in contrast to Y_2O_3, the $Y_2Si_4N_6C$ sintering additive was able to both introduce nitrogen and remove more SiO_2 impurities during the formation of the liquid secondary phase (Li et al., 2018). As a result, the addition of $Y_2Si_4N_6C$ increased the N/O atomic ratio in the secondary phase, which was advantageous for obtaining larger elongated grains, decreased lattice oxygen content, increased Si_3N_4–Si_3N_4 contiguity, and a more devitrified grain-boundary phase in the sintered Si_3N_4 sample. Because of these features, the thermal conductivity of Si_3N_4 ceramic was significantly increased by ~30.4 % from 92 to 120 W/(m·K) after the use of $Y_2Si_4N_6C$ instead of Y_2O_3 as a sintering additive. The binary non-oxide $ZrSi_2$–$MgSiN_2$ as sintering additives (Wang et al., 2020b), which increased the N/O ratio in the liquid phase, delayed densification, and prevented oxygen incorporation. By replacing oxide additives with non-oxide additives, native SiO_2 was eliminated, and a nitrogen-rich liquid was created. This led to the production of pure Si_3N_4 grains, decreased glassy phase, and improved Si_3N_4–Si_3N_4 contiguity. Ultimately, a thermal conductivity of 117.3 W/(m·K) was achieved. **Table 2** summarizes the thermal conductivities of the prepared Si_3N_4 ceramics with the non-oxide sintering additives. When the sample was sintered at 1900 °C for 12 h, no matter what kind of sintering additives were used, the thermal conductivity results could only be increased to about 120 W/(m·K). It was therefore necessary to extend the holding time to further improve the thermal conductivity of the Si_3N_4 ceramics.

3.2 Enhancing thermal conductivity by exploiting grain anisotropy

During the sintering of Si_3N_4 ceramics, there are two stages: α–β Si_3N_4 phase transformation and β-Si_3N_4 grain growth. The α–β phase transformation facilitates the growth of large elongated grains, resulting in a typical bimodal microstructure composed of large elongated grains embedded in a small-grained matrix (Becher et al., 2008; Kitayama et al., 1998a, 1998b, 2006; Suematsu et al., 2005). The fine β-Si_3N_4 grains would lead to increased grain-boundary interface and influence the properties of Si_3N_4 ceramics, thereby the phonon mean free path decreases and suppresses thermal conductivity (Feng and Ruan, 2014). The properties of Si_3N_4 ceramics can be improved by modulating their microstructure, generally the grain size distribution, secondary-phase composition and the β Si_3N_4 grain orientation or texture. An increase in the fraction of large elongated grains also results in numerous grain impingements. These impingements often reduce the

Table 2 Comparison of thermal conductivity results of Si_3N_4 ceramics with non-oxide sintering additives (1: GPs; 2: SRBSN; 3: RSMF-GPs; 4: HPs-GPs).

Reference	Sintering additive	Sintered method	Sintering condition	κ/W/(m·K)
(Hayashi et al., 2001b)	Yb_2O_3:$MgSiN_2$ = 2:5 mol%	1	1900 °C, 48 h	140
(Zhu et al., 2006a)	Y_2O_3:$MgSiN_2$ = 2:5 mol%	1	1900 °C, 12 h	117
(Zhu et al., 2006b)	Y_2O_3:$MgSiN_2$ = 2:5 mol%	2	1900 °C, 12 h	121
(Zhu et al., 2007b)	Y_2O_3:$MgSiN_2$ = 2:5 mol%	2	1900 °C, 12 h	119
(Zhou et al., 2008)	Y_2O_3:$MgSiN_2$ = 2:5 mol%	2	1900 °C, 24 h	133
(Wang et al., 2014b)	LaF_3:MgO = 5:3 wt.%	1	1900 °C, 3 h	97
(Zhu et al., 2014)	Y_2O_3:$MgSiN_2$ = 2:5 mol%	3	1900 °C, 12 h	176
(Hu et al., 2016)	Y_2O_3:MgF_2 = 5:4 wt.%	1	1850 °C, 3 h	82
(Lee et al., 2016)	YbF_3:$MgSiN_2$ = 2:5 mol%	4	1850 °C, 3 h	101
(Liang et al., 2016)	YF_3:MgO = 3:3 wt.%	4	1850 °C, 3 h	75
(Li et al., 2018)	$Y_2Si_4N_6C$:MgO = 2:5 mol%	1	1900 °C, 12 h	120
(Wang et al., 2019)	$ZrSi_2$:MgO = 3:4 mol%	1	1900 °C, 12 h	113
(Wang et al., 2020a)	YH_2:MgO = 3:1.5 wt.%	1	1900 °C, 12 h	123
(Wang et al., 2020b)	$ZrSi_2$:$MgSiN_2$ = 3:4 mol%	1	1900 °C, 12 h	117
(Zhang et al., 2020)	Y_2O_3:$MgSiN_2$ = 3:7 mol%	1	1900 °C, 8 h	117
(Hu et al., 2021)	Y_2O_3:$MgSiN_2$ = 3:5 mol%	1	1890 °C, 3 h	91.9
(Liao et al., 2021)	YF_3:MgF_2 = 6:3 mol%	1	1750 °C, 2 h	69
(Wang et al., 2021)	ZrH_2:MgO = 3:1.5 wt.%	1	1900 °C, 12 h	116
(Fu et al., 2022)	Gd_2O_3:$MgSiN_2$ = 2:2 mol%	1	1900 °C, 12 h	124
(Huang et al., 2022)	$Y_2Si_4N_6C$:MgO = 2:5 mol%	1	1900 °C, 12 h	111.8
(Liu et al., 2023)	Y_2O_3:$MgSiN_2$ = 1:5 wt.%	1	1900 °C, 12 h	106.7

grain diameter locally, forming notch-like features that can reduce the strength of the reinforced grain.

In the late 1990s, researchers chose the tape casting (TCA) and extrusion alignment (EA) processes for the preparation of the green body with β-Si_3N_4 seed, and the samples were sintered by gas pressure (GPs), hot pressure (HPs), or hot isostatic pressing (HIPs) technology (Duan et al., 2017). As shown in **Fig. 5(a)**, by extruding via a die with the desired shape (such as square or circle) in an extrusion machine, rod-like β-Si_3N_4 seed particles can be aligned unidirectionally. The tape casting technology can also quickly prepare large-area ceramic films with high production efficiency, good product consistency, stable performance, and easy to realize continuous and automated preparation (Gutiérrez and Moreno, 2000; Zhang et al., 2006). Additionally, it is an effective method for creating a green body with oriented anisotropic ceramic particles, which results in the creation of textured ceramics, as schematically illustrated in **Fig. 5(b)**. β-Si_3N_4 seed particles that are rod-like and have a unidirectional orientation can form a green body through tape casting. Similar to EA, a slurry containing β-Si_3N_4 seeds should be thoroughly combined, usually using ball milling with nylon balls.

Using the microstructural characteristics of Si_3N_4 ceramics, researchers have prepared anisotropic Si_3N_4 ceramics to improve thermal conductivity (Becher et al., 1998; Sun et al., 1998). Because of the long columnar morphology of β-Si_3N_4, it is possible to obtain the optimum value of thermal conductivity in a certain direction by orienting the grains. For example, (Hirao et al., 1996) added β-Si_3N_4 seeds by tape casting, and the thermal conductivities in parallel and perpendicular to the direction of casting were 121 and 66 W/(m·K), respectively, after holding at 1900 °C for 66 h. As reported by (Watari et al., 1999), the Si_3N_4 ceramics with highly anisotropic were successfully prepared by tape casting of raw α-Si_3N_4 powders with β-Si_3N_4 grain seed particles and Y_2O_3 as a sintering additive, followed by hot isostatic pressing at a temperature of 2500 °C for 2 h under a nitrogen gas pressure of 200 MPa. In **Fig. 6**, large and elongated grains with a diameter of approximately 10 mm and a length of approximately 200 mm comprise the microstructure of Si_3N_4 ceramic. These grains were

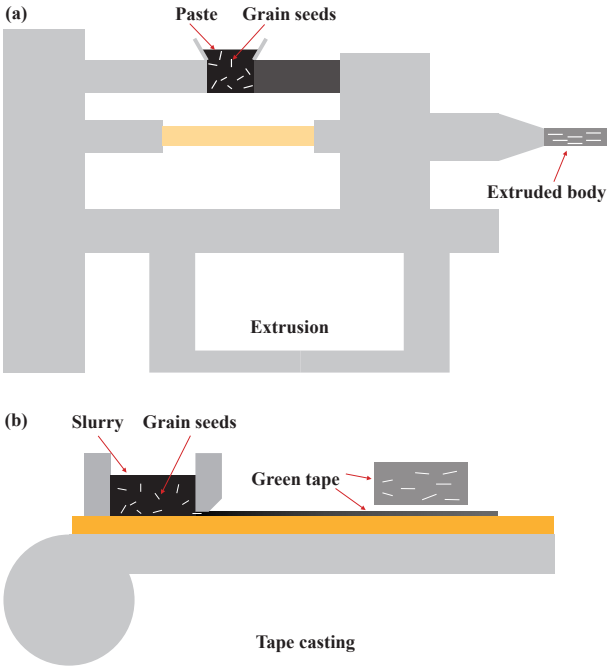

Fig. 5 Schematic illustration of producing Si_3N_4 green body with oriented rodlike β-Si_3N_4 seeds by **(a)** EA and **(b)** TCA techniques. (Original work by the authors.)

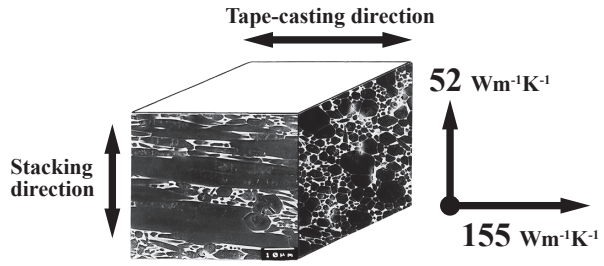

Fig. 6 SEM photographs of the plasma-etched surface and room temperature thermal conductivities of a Si_3N_4 specimen fabricated by tape-casting, hot pressing, and subsequent HIP sintering. Adapted with permission from Ref. (Watari et al., 1999). Copyright 1999, Springer.

heavily oriented toward tape casting. At ambient temperature, the thermal conductivity in this direction was 155 W/(m·K).

Until now, the only way to produce textured and untextured Si_3N_4 with thermal conductivities above 120 W/(m·K) was through an intricate procedure that involved prolonged sintering and annealing at elevated temperatures. However, their expensive fabrication costs and poor dependability make them unsuitable for commercial use. The development of superconducting magnet technologies has led to the use of strong magnetic fields (≥10 T) that allow the crystallographic orientation of ceramic crystals through colloidal processing. Texture development in Si_3N_4 by strong magnetic field alignment (SMFA) using slip casting of α-Si_3N_4 raw powder (SN-E10) and pressureless sintering (Zhu et al., 2008). **Fig. 7** shows the microstructures of β-Si_3N_4 slip cast in a static magnetic field of 12 T **(left)** and Si_3N_4 consolidated in a rotating magnetic field **(right)** (Sakka, 2019). They also obtained highly *c*-axis-textured Si_3N_4 with a thermal anisotropy of 55 % by seeded slip casting in a rotating strong magnetic field (RSMF), β-Si_3N_4 grain has an intrinsic thermal anisotropy of up to 62 % (Zhu et al., 2010a). Fabricating textured Si_3N_4 with the *c*-axis parallel to the thickness direction was made possible by the RSMF technology. By using RSMF technology to slip cast α-Si_3N_4 raw powder with β-Si_3N_4 seeds and Y_2O_3–$MgSiN_2$ as sintering additives, Zhu et al. (2014) proposed a novel method for creating textured Si_3N_4 with a high thermal conductivity of 176 W/(m·K) along the grain alignment direction. This was followed by gas-pressure sintering at 1900 °C for 12 h.

High-resolution thermos-reflectance microscopy measurements were performed at five frequencies on rod-shaped Si_3N_4 grains in ceramic (Li et al., 1999). The heat diffusion model takes account of the coating and coating/

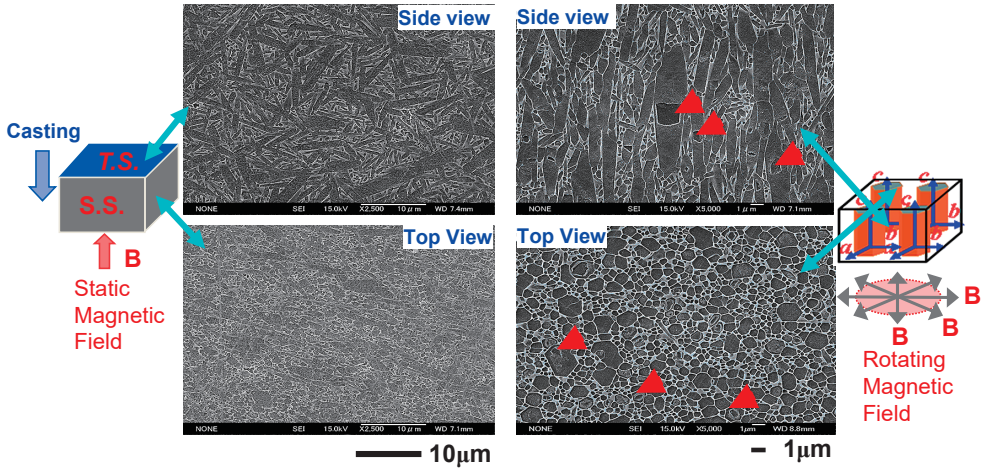

Fig. 7 SEM microstructures of β-Si_3N_4 slip-cast in a static magnetic field of 12 T **(left)** and β-Si_3N_4 consolidated in a rotating magnetic field **(right)** after sintering at 1800 °C for 5 h. Reprinted from Ref. (Sakka, 2019) under the terms of the CC-BY 4.0 license. Copyright: (2019) The Author, published by Hosokawa Powder Technology Foundation.

substrate resistance. **Fig. 8(a)** shows a schematic of the thermal microscope. The heating laser was a semiconductor laser. With a frequency of 1 MHz, a round form of 8 um in diameter, a wavelength of 808 nm, and a maximum output power of 150 mW, the heating laser was sinusoidally modulated. The probe laser, which was coaxially aligned with the heating laser, had a diameter of 3 um, a wavelength of 658 nm, and an output power of 35 mW. The thermal microscope and chamber were maintained at 24 + 1 °C. The specimen surface was polished to a mirror finish and then coated with a molybdenum film (100 + 5 nm thick) in an Ar gas atmosphere at a pressure of 6 Pa at room temperature.

The temperature modulation of the surface was detected as a reflectance signal by the probe laser, which allowed the measurement of the phase lag, or the interval between the periodic heating and the reflectance signal. As a result, the absorbed heat in the molybdenum film diffuses into the specimen, and the local temperature at the heated surface

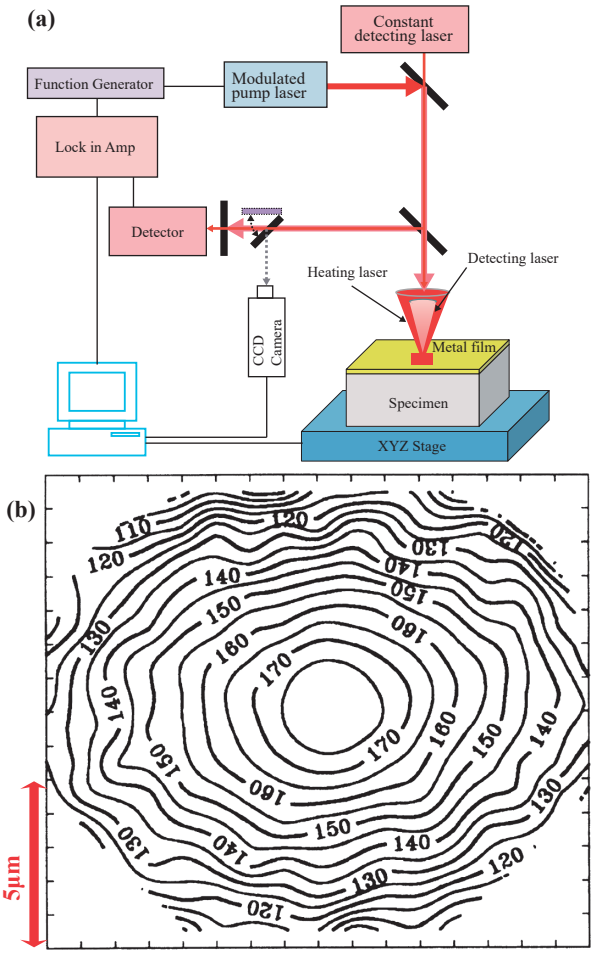

Fig. 8 **(a)** Schematic diagram of thermos-reflectance microscopy (Lee et al., 2008), reprinted with permission from J-STAGE "open access". **(b)** Contour lines of the phase of the thermos-reflectance signal on very large β-Si_3N_4 grain. Strong heat flow is observed along the *c*-axis of β-Si_3N_4 grain. Adapted with permission from Ref. (Li et al., 1999). Copyright 1999, Elsevier.

changes proportionately with the sinusoidal heating. The thermal coefficient of the sample was estimated using the measured phase lag and calibration curves derived from standard materials such as SiC, AlN, Si, and Pyrex. With matching conductivities of 69 and 180 W/(m·K), the primary diffusivities obtained in individual grains are 0.32 $cm^2 \cdot s^{-1}$ along the *a*-axis and 0.84 $cm^2 \cdot s^{-1}$ along the *c*-axis. It is discovered that the thermal anisotropy inside individual Si_3N_4 grains is intrinsic and unrelated to their elongated shape.

In the same year, the textured Si_3N_4 was obtained by extrusion with β-Si_3N_4 whiskers, followed by gas-pressure sintering at 1900 °C for 4 h and subsequent annealing at 2200 °C for 16 h at a nitrogen pressure of 30 MPa (Akimune et al., 1999). This textured Si_3N_4 exhibited the highest thermal conductivity of 162 W/(m·K) along the grain alignment direction. The crystal structure was analyzed using Raman spectroscopy to determine whether micro-stacking faults in the β-Si_3N_4 phase were caused by structural flaws in the Si_3N_4 grains. Using this method, the existence or lack of a 514–520 cm^{-1} peak indicates the existence or non-existence of stacking defects of this type. In orientation-controlled Si_3N_4, a large grain diameter and high thermal conductivity can be achieved only in the β-Si_3N_4 phase. In contrast, even though the heat treatment process was carried out at the same temperature, the grain diameter was smaller and stacking defects appeared in the β-Si_3N_4 phase of gas-pressure hot-pressed Si_3N_4. It was discovered that phonon-impurity scattering, which is caused by structural flaws in the crystal grains, decreases heat conductivity. This suggests that to achieve high heat conductivity, structural flaws in the grains must be removed. According to the study, structural investigations using Raman spectroscopy may be a useful method for identifying these types of flaws.

3.3 Effects of grain lattice defects and microstructure

The main reasons affecting the thermal conductivity of Si_3N_4 ceramics were analyzed from the viewpoint of ceramic microstructure (Kitayama et al., 1999b). The thermal conductivity of β-Si_3N_4 is predicted to decrease rapidly as the grain-boundary film thickness increases within a few tenths of a nanometer and to initially increase steeply with increased grain size before reaching nearly constant values, according to calculations based on a basic modified Wiener's model for thermal conductivity of a composite material. The "average" thickness of the grain-boundary film was significantly higher than the equilibrium thickness due to the faceted structure of the β-Si_3N_4 crystal. The results show that the thermal conductivity of β-Si_3N_4 cannot be increased by grain growth alone, both in theory and in practice.

According to **Fig. 9(a)**, when the mean grain size is

plotted on a logarithmic scale, a good straight line can be drawn for the plots of the experimental data, suggesting an apparent exponential dependence of thermal conductivity on the mean grain size. And **Fig. 9(b)** illustrates that the thickness of the grain-boundary coating, which varies within a few tenths of a nanometer, considerably affects the thermal conductivity of β-Si_3N_4. This study also demonstrates how the arrangement of anisotropic β-grains, which alter the quantity of thin films per unit thickness, can lead to anisotropic thermal conductivity. This study clarified the connection between β-Si_3N_4 thermal conductivity and other microstructural elements, showing that grain growth by itself cannot increase the material's thermal conductivity over a set of critical grain sizes.

With respect to β-Si_3N_4, several crystal defects were identified in the grains. Thus, dense β-Si_3N_4 with different Y_2O_3/SiO_2 additive ratios were obtained by hot pressing, sintering, and annealing. The grain-boundary phase composition dictates the lattice oxygen content of β-Si_3N_4 (Kitayama et al., 2000). Using the hot-gas extraction approach, they were able to determine the oxygen content of Si_3N_4 crystal lattices and discovered that, depending on the additive compositions, the oxygen content of Si_3N_4 grains ranges from 0.158 to 0.258 weight percent. When both $Y_{20}N_4Si_{12}O_{48}$ and $Y_2Si_3N_4O_3$ are present in the grain-boundary phase, the lattice oxygen concentration is the lowest. The grain-boundary phase increases when excess Y_2O_3 is added, but the lattice oxygen concentration does not decrease. Therefore, based on the quantity of oxygen impurities in the Si_3N_4 raw powder, an ideal Y_2O_3 addition amount is found to provide the maximum κ value in β-Si_3N_4. Additionally, they discovered nitrogen vacancies, which bind to dissolved oxygen atoms, using electron spin resonance (ESR) to assess the concentration of vacancies in the Si_3N_4 grains. For example, during sintering, the impurity oxygen takes the place of nitrogen atoms in the crystal lattice to form the oxygen occupancy (O_N^+), which leads to the creation of silicon vacancies (V_{Si}^{4-}) due to the charge equilibrium, and according to the above mention of the effect of defects on phonon scattering, it can be seen that lattice defects significantly reduce the mean free range of phonons.

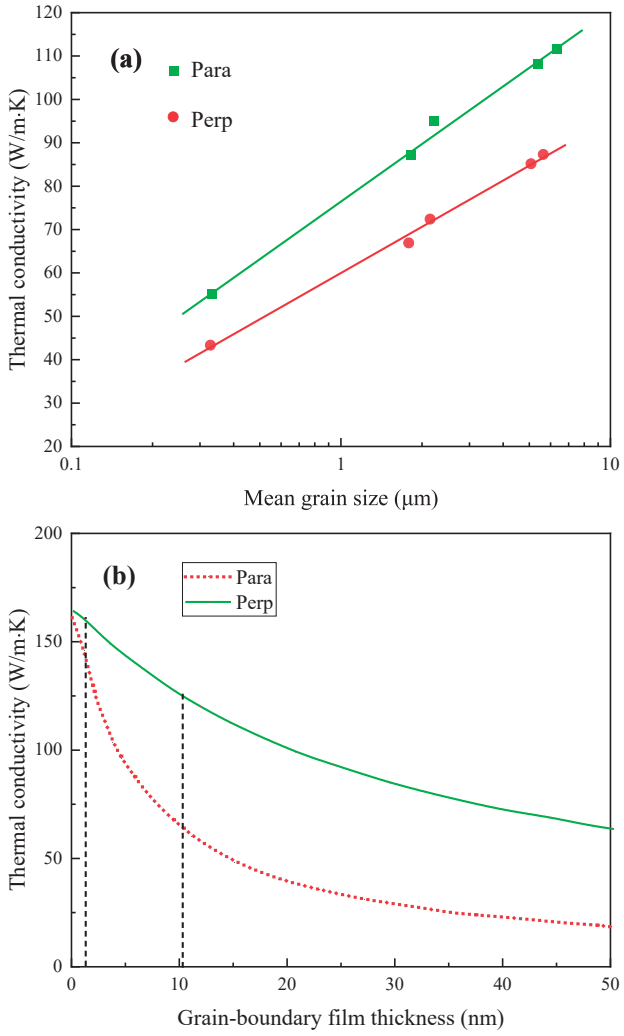

Fig. 9 **(a)** Relationship between mean grain sizes and thermal conductivities of β-Si_3N_4 sintered bodies; **(b)** Effect of grain-boundary thickness on thermal conductivity of β-Si_3N_4 for d = 1 mm, l = 5 mm (R = 5), and x = 6 %. Adapted with permission from Ref. (Kitayama et al., 1999b). Copyright 1999, John Wiley & Sons.

By analyzing the Si_3N_4 grains in a sintered specimen with a conductivity value of 100 W/(m·K) (Yokota and Ibukiyama, 2003), they found that the grains consistently contained about 200 ppm Al by weight. The raw powders were the source of the Al contamination. Aluminum and dissolved oxygen constitute a single type of point defect. In 2002, the energy transfer in α- and β-Si_3N_4 single crystals was simulated using a molecular dynamics approach. Using the simulation data, the Green-Kubo formulation was applied to calculate the thermal conductivity of the single crystals. As a function of temperature, it is known that the thermal conductivities of α-Si_3N_4 crystals along the a and c axes are 105 and 225 W/(m·K), respectively; and the thermal conductivities of β-Si_3N_4 crystals along the a and c axes are 170 and 450 W/(m·K), respectively, and the results of the data indicate that the Si_3N_4 crystals have a higher thermal conductivity, which is suitable for the preparation of high-permeability Si_3N_4 ceramics. The results show that Si_3N_4 crystals have high thermal conductivity, which lays a theoretical foundation for the preparation of high thermal conductivity Si_3N_4 ceramics and provides a theoretical basis for the improvement of the thermal conductivity of Si_3N_4 ceramics (Hirosaki et al., 2002). In **Fig. 10**, the data demonstrate a definite tendency for thermal conductivity to increase with decreasing lattice oxygen content, regardless of the sintering additives and sintering techniques. Even though the manufactured Si_3N_4's lattice oxygen concentrations were similar, their thermal conductivities may differ depending on the sintering additives and techniques used. This was brought about by a few

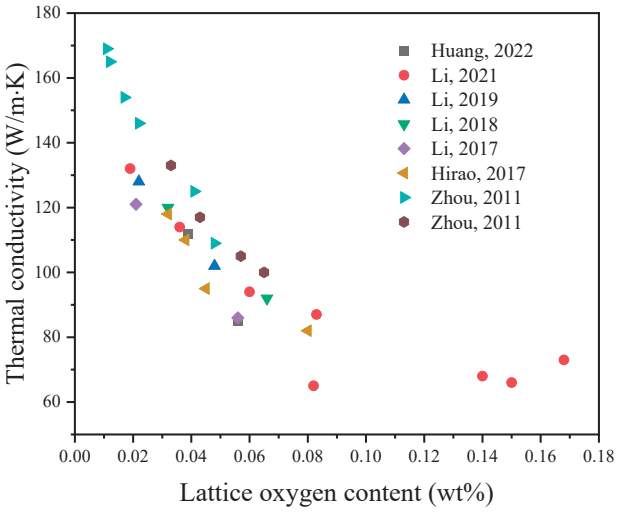

Fig. 10 Relationship between thermal conductivity and lattice oxygen content (Hirao et al., 2017; Huang et al., 2022; Li et al., 2018, 2019, 2021; Zhou et al., 2011). (Original work by the authors.)

microstructural elements (grain size, grain boundary phase, grain orientation, etc.) (Hayashi et al., 2001a; Hirao et al., 2001; Kitayama et al., 2000; Yokota and Ibukiyama, 2003; Zhou et al., 2011, 2015).

However, as illustrated in **Fig. 11**, these effects paled in comparison with the impact of the lattice oxygen content on thermal conductivity. The β-Si_3N_4 ceramics were sintered with various rare-earth (RE = La, Nd, Gd, Y, Yb, and Sc) oxides (Kitayama et al., 2001). The mean grain size increased while the lattice oxygen content decreased; hence, the thermal conductivity increased with the decreasing ionic radius of the rare-earth element. **Fig. 11** shows the relationship between the ionic radii of rare-earth oxide additives and lattice oxygen contents of β-Si_3N_4. The results from a sample sintered with La_2O_3 at 1850 °C for 4 h are not included in this figure because it contains a considerable amount of the α-phase, which has an oxygen content of roughly 0.83 weight percent. The oxygen content in the A crystal lattice approaches a constant value below the decreasing ionic radii of La, Nd, and Gd. As the rare-earth element's ionic radius decreases, the mean grain size increases and the lattice oxygen concentration decreases, increasing the thermal conductivity (diffusivity).

It is well known that the phase transformation and Ostwald ripening of Si_3N_4 proceed via solution–reprecipitation in the liquid phase that is formed at high temperature by the reaction between sintering additives, Si_3N_4, and SiO_2 derived from the oxygen impurity of the raw powder. It is true that the viscosity and wetting behavior of the liquid phase affect the kinetics of these processes. However, the interfacial reaction rate between the prismatic facet of the β-Si_3N_4 crystal and the liquid phase is the most important factor affecting the performance of this material (Kitayama et al., 1999a). It was shown that when the ionic radius of the rare-earth element decreases, the grain development of β-Si_3N_4

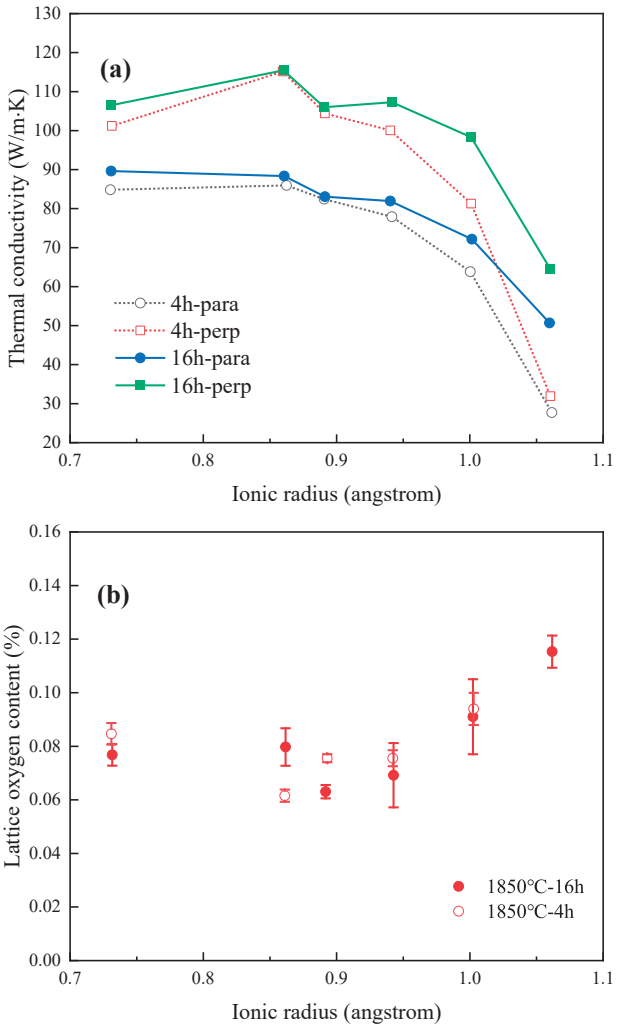

Fig. 11 Relationship between thermal **(a)** conductivities (the "para" and "perp" specimens of β-Si_3N_4 sintered bodies.), **(b)** lattice oxygen concentrations of β-Si_3N_4 and the ionic radii of rare-earth oxide additions. Adapted with permission from Ref. (Kitayama et al., 2001). Copyright 2001, John Wiley & Sons.

changes from being interfacial reaction controlled to diffusion controlled. Subsequently, the activation energy of the interfacial reaction was observed to decrease linearly with decreasing ionic radius. This explains why the mean grain size (mean grain width) grows with decreasing ionic radius of rare-earth ions and why the phase change rate of a sample sintered with La_2O_3, the largest among rare-earth ions, is particularly sluggish.

For each of the five sintering additive types, the high-angle annular dark-field scanning transmission electron microscopy (HAADF-STEM) images in **Fig. 12** show a contact between the intergranular phase and a Si_3N_4 matrix grain (Ziegler et al., 2004). The images verify that the interface with the intergranular phase, namely, with open hexagonal rings, is where the Si_3N_4 crystal structure finishes (Ziegler et al., 2003). The *Z*-contrast in the images—which makes heavier atoms appear brighter—proves that heavy atoms are attached. The heavy components do, in fact,

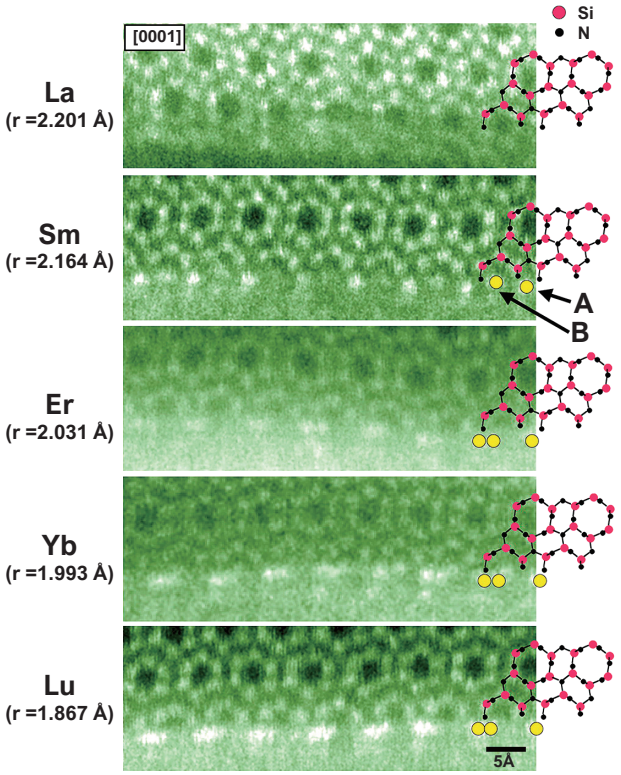

Fig. 12 The matrix grain is oriented along the [0001] zone axis in the STEM images of La-, Sm-, Er-, Yb-, and Lu-doped Si_3N_4, allowing the open Si_3N_4 crystal structure to be clearly seen at the atomic level, with its prismatic plane facing the amorphous intergranular phase. Adapted with permission from Ref. (Ziegler et al., 2004). Copyright © 2004, The American Association for the Advancement of Science.

segregate to the intergranular phase, as confirmed by concurrent large-area EELS measurements on these contacts. As a result, the heavy atoms and their atomic locations are in fact related to the brilliant spots shown in the images. For all the rare-earth elements (La, Sm, Er, Yb, and Lu) studied here, the atomic attachment at such interfaces varies. The Si_3N_4 matrix grain and La atoms do not appear to be connected in any particular or regular way in the STEM images of the sample containing La.

Although La atoms are present in the intergranular phase, they do not align into atomic columns that enhance contrast (Shibata et al., 2004). Moreover, at this magnification, no lateral atomic ordering can be observed. Prior studies have demonstrated the presence of spots with high and low concentrations of La atoms along the intergranular phase, indicating fluctuations in the La atom distribution. Because of their considerable separation, regions with high La concentration cannot be linked to a specific atomic site along the interface. Simultaneous theoretical calculations aimed at identifying particular atomic locations are beneficial. Nevertheless, consistent with the current findings, unassisted STEM images do not clearly show a periodic atomic site for La atom attachment.

3.4 Sintering of reaction-bonded Si_3N_4

The maximum achievable thermal conductivity of Si_3N_4 ceramics is limited because even the highest quality commercial powder for Si_3N_4 starting powders has more than 1 wt% oxygen present in the lattice and on the surface. Using a starting powder with less oxygen will increase the upper limit to a greater extent. Inspired by this notion, the researcher proposed the preparation of high thermal conductivity Si_3N_4 using the well-known reaction-bonded silicon nitride (SRBSN technique), which fabricates Si_3N_4 ceramics from a Si starting powder rather than a Si_3N_4 powder (Zhu et al., 2006b).

In consideration of the fact that Si powders containing much less oxygen and metallic impurities than Si_3N_4 powders are commercially available due to the advancement of the modern semiconductor industry. This approach involves two processing steps. To nitride and transform it into a porous Si_3N_4 compact, a Si compact made of Si powder and sintering additives is first heated to a temperature close to the melting point of Si (1414 °C) in a nitrogen atmosphere. Subsequently, the nitrided compact was heated to an elevated temperature below the Si_3N_4 breakdown temperature. This process facilitates the densification of porous Si_3N_4, resulting in the formation of dense Si_3N_4 ceramics. Compared to the sintering of Si_3N_4 (SSN) method, Si raw powders are typically less expensive than Si_3N_4 raw powders, which is why the SRBSN method has long been recognized as an affordable processing method for creating Si_3N_4 ceramics. Nonetheless, the reason for employing the SRBSN technique to create Si_3N_4 ceramics with good thermal conductivity was that it allowed Si powders with less oxygen than even premium Si_3N_4 powders to be used as the initial ingredients. Controlling the oxygen level of the post-sintered Si_3N_4 is advantageous because the entire process, from nitridation to post-sintering, can be carried out continuously without exposing the compacts to air.

Zhou et al. obtained the highest thermal conductivity of 177 W/(m·K) for Si_3N_4 by nitriding combined with SRBSN at 1900 °C for 60 h and cooling at a rate of 0.2 K/min using a raw material of high-purity Si with low oxygen content. Since the purity of silicon powder (e.g., oxygen content, metal impurities, etc.) is much higher than that of Si_3N_4 powder, the lattice defects of Si_3N_4 ceramics prepared using SRBSN are reduced accordingly. As shown in **Fig. 13(a)**, the reduction in grain boundary content substantially reduced the scattering of phonons at the grain boundary locations, thus increasing the thermal conductivity of the material. Combined with the compositional analysis (**Fig. 13(b)**), the Y, Mg, and O elements introduced by the sintering aids were mainly distributed at the thinner grain boundary locations. Si_3N_4 with a high thermal conductivity of about 180 W/(m·K), a bending strength of 600 MPa, and a high fracture toughness of 11 MPa·$m^{1/2}$ has been developed by this method (Hirao et al., 2017).

Zhou altered the nitriding conditions by increasing the reducing atmosphere in the reaction zone and increasing the heating rate. This resulted in a greater β:α-Si_3N_4 ratio, which could contribute to increased thermal conductivity. This assumption is based on the fact that numerous studies conducted since the 1970s have demonstrated that α-Si_3N_4 can accommodate varying amounts of oxygen in its lattice (Wang et al., 1996). However, until Kitayama et al.'s measurement in 1999, there was no information available regarding the oxygen dissolution in β-Si_3N_4, which showed that the oxygen dissolved in a β-Si_3N_4 crystal lattice is significantly less than the values reported for most α-Si_3N_4. This implies that when a reaction-bonded Si_3N_4 (RBSN) is formed by nitriding Si, a subsequent β-Si_3N_4 crystal may accommodate a lower amount of lattice oxygen than a resultant α-Si_3N_4 crystal. If this is the case, then steps should be taken to improve the β phase's production during nitridation to lower the overall lattice oxygen concentration and raise the prepared SRBSN material's thermal conductivity.

Based on the above research, our group adjusted the nitridation technology. The Si compacts were nitrided in a graphite tube furnace with a mixed gas (N_2:H_2 = 95:5) at 1400 °C for 2 h and then further heated to 1450 °C for 6 h. As expected, the phase content ratios β/(α + β) of almost all samples exceeded 90 % (**Fig. 14(a)**). The ratios were usually lower than 15 % as the Si compacts were usually nitrided at 1400 °C for 8 h in our previous experiments. This result is attributed to the formation of the α-Si_3N_4 phase, which was favored at a reaction temperature below the melting point of silicon. As shown in **Fig. 14(b)**, when Er_2O_3–MgO was used as the sintering aid, a large number of rod-like crystals appeared in the cross-sectional microstructure of the nitrided samples, which is consistent with the result of the ratio of β/(α + β) in **Fig. 14(a)**. Meanwhile, it can be seen that the liquid phase of the sintering aid phase is initially formed inside the nitrided samples in **Fig. 14(b)**, but the distribution is not homogeneous, and defects such as pores will be left behind during the subsequent sintering process, which will result in a decrease in the thermal conductivity of the material and the Weibull modulus in the mechanical properties becomes lower.

According to **Table 3**, it also can be seen when the sample was sintered at 1900 °C for 12 h, the thermal conductivity results still increased to about 120 W/(m·K). However, silicon powder is derived from the crystalline silicon for photovoltaic modules, which has a greater yield and lower cost, so SRBSN technology has a greater advantage in the preparation of high thermal conductivity Si_3N_4 ceramics. However, the technology is still faced with the following difficulties:

1) Due to the very high flatness of the green bodies, the nitrogen pressure distribution seriously affects the diffusion rate of nitrogen on the surface of silicon particles, and it is very easy for the phenomenon of nitriding insufficiency to occur. The residual silicon reduces the thermal conductivity and mechanical properties of Si_3N_4 ceramics.
2) Silicon powder cast film is a nearly two-dimensional planar material, and it is necessary to control the nitrided bodies in the α/β-Si_3N_4 ratio and other uniformity properties to avoid deformation, cracking, and

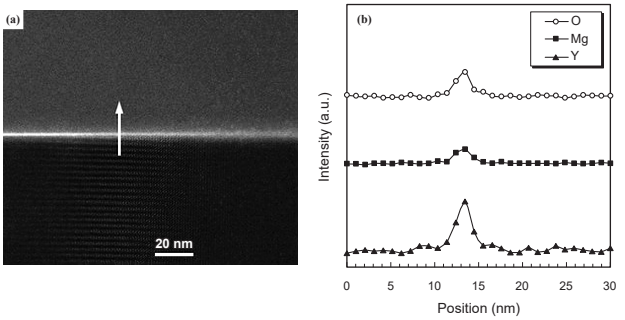

Fig. 13 **(a)** HAADF-STEM image showing the boundary between two adjacent Si_3N_4 grains; **(b)** Compositional line profiles across the grain boundary shown in **(a)**. Adapted with permission from Ref. (Zhou et al., 2011). Copyright 2011, John Wiley and Sons.

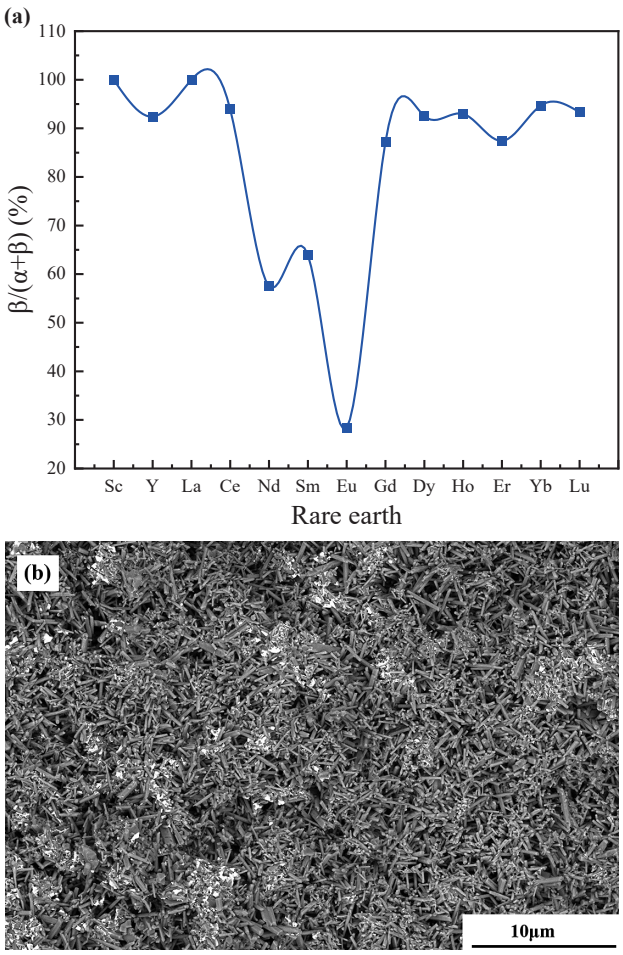

Fig. 14 **(a)** the ratio of β/(α + β) of nitrided Si compacts; **(b)** SEM photograph of nitrided sample with Er_2O_3 as sintering additive. Adapted with permission from Ref. (Duan et al., 2020). Copyright 2019. Elsevier.

Table 3 Comparison of thermal conductivity of the SRBSNs.

Reference	Sintering additive	Nitriding condition	Sintering condition	κ/W/(m·K)
(Zhu et al., 2006b)	Y_2O_3:$MgSiN_2$ = 2:5 mol%	1400 °C, 8 h	1900 °C, 12 h	121
(Zhu et al., 2007a)	Y_2O_3:$MgSiN_2$ = 2:5 mol%	1400 °C, 8 h	1900 °C, 24 h	133
(Zhu et al., 2007b)	Y_2O_3:$MgSiN_2$ = 2:5 mol%	1400 °C, 8 h	1900 °C, 12 h	119
(Zhou et al., 2008)	Y_2O_3:MgO = 2:5 mol%	1400 °C, 8 h	1900 °C, 24 h	133
(Zhou et al., 2011)	Y_2O_3:MgO = 2:5 mol%	1400 °C, 4 h	1900 °C, 120 h	177
(Kusano et al., 2013)	Y_2O_3:$MgSiN_2$ = 2:5 mol%	1400 °C, 8 h	1900 °C, 6 h	82
(Golla et al., 2014)	Y_2O_3:MgO = 3.5:1.5 wt.%	1450 °C, 2.5 h	1950 °C, 3 h	89.6
(Kusano et al., 2014)	Y_2O_3:$MgSiN_2$ = 2:5 mol%	1400 °C, 8 h	1900 °C, 6 h	91.9
(Kim et al., 2017)	Y_2O_3:Sc_2O_3 = 1:3 mol%	1450 °C	1900 °C, 12 h	116.9
(Li et al., 2017)	Y_2O_3:MgO = 2:5 mol%	1400 °C, 6 h	1900 °C, 12 h	121
(Duan et al., 2020)	Er_2O_3:MgO = 2:5 mol%	1450 °C, 6 h	1900 °C, 2 h	90

other defects caused by inconsistent shrinkage rates during the sintering process.

3) The silicon powder cast film nitriding time is long, and some of the added sintering additives will have a certain volatile loss, which in turn affects the density of the sintered body.

3.5 New routines for improving thermal conductivity

At the present stage, research to improve the thermal conductivity of Si_3N_4 mainly focused on the selection of oxygen-free sintering additives and the choice of SRBSN process technology, but it can be seen from the above research progress that the ceramic thermal conductivity is almost stagnant under the same preparation conditions for 120 W/(m·K). Considering the important influence of lattice oxygen defects on the performance of the Si_3N_4 ceramics, the researchers further conducted research into the elimination of lattice oxygen.

The researchers examined how the thermal conductivity of β-Si_3N_4 ceramics was affected by the embedding conditions (Zhu et al., 2006a). It was discovered that although the embedment affected the weight loss, crystalline secondary phase, and microstructure, it did not influence densification. The heat conductivity increased regardless of particle size and increased linearly with weight reduction. The weight loss is suppressed, and the thermal conductivity is lowered because of the full embedment and the greater number of sintered samples. The thermal conductivity increased significantly from 96 to 117 W/(m·K) under ideal conditions. the elimination of lattice oxygen is the cause of the increased thermal conductivity:

$$Si_3N_4(s) + 3SiO_2(l) = 6SiO(g) + 2N_2(g)$$

Then, in 2019, Li added a small amount of carbon to the

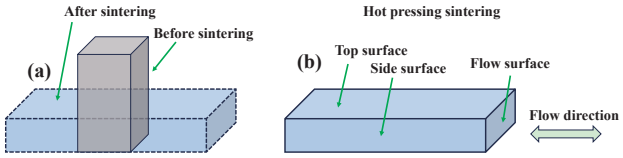

Fig. 15 **(a)** The comparison diagram of the sample before and after sintering; **(b)** The one-dimensional flowing sintered sample (Li et al., 2024). Copyright 2024, John Wiley & Sons.

Si_3N_4. During the first-step sintering, the carbothermal reduction process significantly reduced the oxygen content and increased the N/O ratio of the intergranular secondary phase, resulting in the precipitation of $Yb_2Si_4O_7N_2$ crystalline phase, higher β-Si_3N_4 content and larger rod-like β-Si_3N_4 grains in the semi-finished Si_3N_4 sample. Due to the further carbothermal reduction of the oxynitride secondary phase following the second-step sintering, the final dense Si_3N_4 product exhibited tighter Si_3N_4–Si_3N_4 interfaces, coarser elongated grains, lower lattice oxygen content, and a more devitrified intergranular phase. As a result, the use of carbon allowed the thermal conductivity of Si_3N_4 ceramic to improve significantly from 102 to 128 W/(m·K), or roughly 25.5 %.

The Si_3N_4 exhibiting enhanced thermal conductivity and flexural strength was sintered by hot-pressing flowing sintering (HPFS) method (**Fig. 15**) (Li et al., 2024). As the strain increased from 67 % to 167 %, the mean grain diameter of Si_3N_4 with $MgSiN_2$ as an additive increased by 49 %, reaching 1.36 ± 0.6 μm. The addition of $MgSiN_2$–Y_2O_3 resulted in a significantly stronger texturing degree and smaller grain diameter in Si_3N_4 compared to the incorporation of $MgSiN_2$ alone. The thermal conductivity of Si_3N_4 with added $MgSiN_2$–Y_2O_3 increased to 109.1 W/(m·K) in the flow direction, and the flexural strength reached a maximum value of 1250.8 ± 39 MPa in the hot-pressing direction. The increase in flexural strength was due to the

Table 4 Comparison of thermal conductivity results of PLs (5: PLs; 6: HPs; 7: SRBSN-PLs).

Reference	Sintering additive	Sintered method	Sintering condition	κ/W/(m·K)
(Matovic et al., 2004)	$LiYO_2$ = 5 wt%	5	1650 °C, 8 h	38
(Wasanapiaenpong et al., 2006)	SiO_2:MgO:Y_2O_3 = 3:3:5 wt%	5	1650 °C, 2 h	34
(Jiang et al., 2011)	$MgSiN_2$ = 4.76 wt%	6	1750 °C, 12 h	129
(Kaidash et al., 2014)	Al_2O_3:Y_2O_3:ZrO_2 = 2:5:5 wt%	5	1750 °C, 2 h	25
(Guo et al., 2016)	ZrO_2:MgO:Y_2O_3 = 7.4:4.4:3.5 wt%	7	1835 °C, 4 h	66.5
(Duan et al., 2018)	MgO:TiO_2 = 5:5 wt%	5	1780 °C, 2 h–1600 °C, 8 h	60
(Duan et al., 2019)	TiO_2:Y_2O_3:MgO = 4:3:2 wt%	5	1810 °C, 4 h–1550 °C, 6 h	74
(Lu et al., 2020)	MgO:Y_2O_3 = 3:6 wt%	5	1800 °C, 4 h	71.5
(Kong et al., 2021)	MgO:Y_2O_3 = 3:3 wt%	5	1800 °C, 6 h	75.6
(Luo et al., 2021)	MgO:LiF = 7:3 wt%	5	1620 °C, 3 h	47.6
(Kumar et al., 2022)	Y_2O_3 + MgO + ZrO_2 = 11 wt%	5	1650 °C, 1 h	50
(Duan et al., 2023)	TiO_2:Y_2O_3:MgO = 1:2:5 mol%	5	1800 °C, 2 h–1700 °C, 2 h	68.5

reduction in internal defects in the material as a result of extrusion deformation. In addition, texturing also decreased collisions during grain growth, which prevented the generation of clusters of large grains.

Low-temperature liquid-phase sintering is an effective method for reducing the preparation cost of Si_3N_4 ceramics. Several sintering additives have been reported in literature, e.g. $LiYO_2$ (Lee, 2010; Matovic et al., 2004), $FeSi_2$ (Wang et al., 2017), Li-exchanged zeolite (Matovic and Boskovic, 2004), magnesia and ceria (Yang et al., 1998) and cordierite (Park et al., 2012). Pressureless sintering (PLs) is currently a common method for preparing non-oxide ceramics, including SiC, AlN, etc., which can be sintered on shaped and large ceramics with high efficiency. Si_3N_4 ceramics can also be prepared via pressureless sintering using appropriate low-temperature sintering additives. By using ZrO_2, MgO, Y_2O_3 sintering additives system, sintered at 1835 °C for 4 h, the fracture toughness and thermal conductivity were 7.0 ± 0.5 MPa·$m^{1/2}$ and 66.5 W/(m·K), respectively (Guo et al., 2016). To prepare dense Si_3N_4 ceramics, high sintering additive contents were needed for effective sintering; thus, the resulting thermal conductivity was too low to satisfy the requirements. Nowadays, choosing suitable additives with low charging content is a possible way to improve thermal properties through pressureless sintering. Our previous work showed that with the addition of TiO_2–MgO as sintering additives, the samples exhibited high mechanical properties; the flexural strength reached 668 MPa after 2 h of sintering at 1750 °C, and the thermal conductivity was 55 W/(m·K) with 10 wt% sintering additives and further increased to 60 W/(m·K) after 8 h of annealing at 1600 °C (Duan et al., 2018). The impurity phases formed by sintering additives significantly influence the properties of Si_3N_4 ceramics seriously (Kusano et al., 2014; Kusano et al., 2013). The annealing treatment has a clear influence on the microstructure, thermal, and mechanical properties of the sintered Si_3N_4 ceramic (Chen et al., 2020). In particular, the grain size, distribution of the impurity phases, and surface microstructure all changed obviously (Yoshida et al., 2011; Zhang et al., 2020). Therefore, to realize the low-temperature sintering of high-performance silicon nitride ceramics, sintering additives with low-temperature eutectic points with SiO_2 are selected, which can produce a sufficient liquid phase at low temperature to promote densification; at the same time, other components are added to regulate the microstructure of the silicon nitride ceramics. The results of the low-temperature sintering study are compared in **Table 4**.

4. Conclusion and outlook

Before 1995, Si_3N_4 ceramics were almost applied as structural ceramics because its theoretical thermal conductivity was considered to reach 170 and 450 W/(m·K). The thermal conductivity of Si_3N_4 ceramics began to soar, and researchers not only adjusted the sintering additives but also took advantage of the anisotropic characteristics of the Si_3N_4 grains to increase the thermal conductivity to about 150 W/(m·K). Since 1999 to 2001, Kitayama successively proposed two major factors affecting Si_3N_4 ceramics, namely, the structure and lattice oxygen defects, to improve the thermal conductivity of Si_3N_4 ceramics to clarify the research ideas, so the new oxygen-free sintering additives as well as the rapid development of the SRBSN technology, the thermal conductivity has been reached about 180 W/(m·K). In recent years, the study of the thermal conductivity of Si_3N_4 has focused on the above two

aspects, and the thermal conductivity level has not been further studied. At the same time, researchers began to develop Si_3N_4 ceramics with high thermal conductivity and high strength Si_3N_4 ceramics through rapid preparation to realize their application value.

With the rapid development of the new energy-based automobile industry, the thermal conductivity of Si_3N_4 ceramics is also increasing, while the preparation technology is also being updated. At present, Si_3N_4 ceramic substrates are currently used in new energy electric vehicles and other fields. The main high thermal conductivity Si_3N_4 ceramic substrate preparation manufacturers, including Japan's Toshiba, Maruwa, and other companies, use Si_3N_4 powder as raw material to obtain a thermal conductivity of Si_3N_4 ceramic substrate greater than 85 W/(m·K), and at the same time have excellent mechanical properties, such as the Maruwa products of thermal conductivity and flexural strength of 90 W/(m·K) and 800 MPa, respectively. While the JFC combined with the reaction of the heavy sintering of Si_3N_4 ceramic substrate, the material exhibits higher thermal conductivity and mechanical properties to meet the future demand for higher applications. The material exhibits higher thermal conductivity and mechanical properties, which can meet the demands of higher applications in the future.

A new generation of Si_3N_4 ceramic substrates with high thermal conductivity has been developed up to 120 W/(m·K). The products from different companies were obtained, and the cross-surface microstructures were characterized by scanning electron microscopy (SEM; Magellan 400, FEI Co., Hillsboro, OR, USA). The comparison of the material microstructure can be seen in **Fig. 16**, the sample with higher thermal conductivity (120 W/(m·K)) has a larger grain size, so in the cycling process is more prone to cracking phenomenon, and then insulation breakdown, so how to ensure that there is no abnormally large grains within the material under the conditions of the rapid increase in the thermal conductivity of Si_3N_4 ceramics, is still the product breakthroughs of the key lies. According to the factors affecting the thermal conductivity, improving the lattice purity is almost the only choice. The main means include improving the purity of raw materials and auxiliary materials, extending the holding time, changing the sintering atmosphere, and so on. Regarding raw material impurity content including metal impurities and oxygen content, etc., powder speed treatment is the main way to reduce the impurity content, such as HF solution can effectively reduce Fe, Cr, and O impurities, HNO_3 solution can remove Ca impurity, a mixture of the two solutions can effectively reduce Al impurity, but in the process of the production of reagents, it will bring a certain amount of environmental problems. When selecting high-purity silicon powder as raw materials, it is necessary to solve the problems mentioned in **Section 3.4**. In the selection of auxiliary materials, an oxygen-free sintering additive should be selected. In addition, the control of debonding and sintering atmosphere is an important way to reduce impurities within, for example, in the selection of silicon powder as raw materials, the selection of N_2:H_2 mixture gas can effectively remove the SiO_2 film on the surface of the silicon powder. The reaction mechanism mainly includes the following: 1) H_2 removes the SiO_2 film on the surface of Si, increasing the nitridation rate; 2) N_2 chemisorbed on the surface of Si particles, promoting the generation of Si_3N_4 nuclei at the initial stage; 3) the reactants (Si and N_2) diffuse on the surface of the nuclei to promote the nitridation reaction,

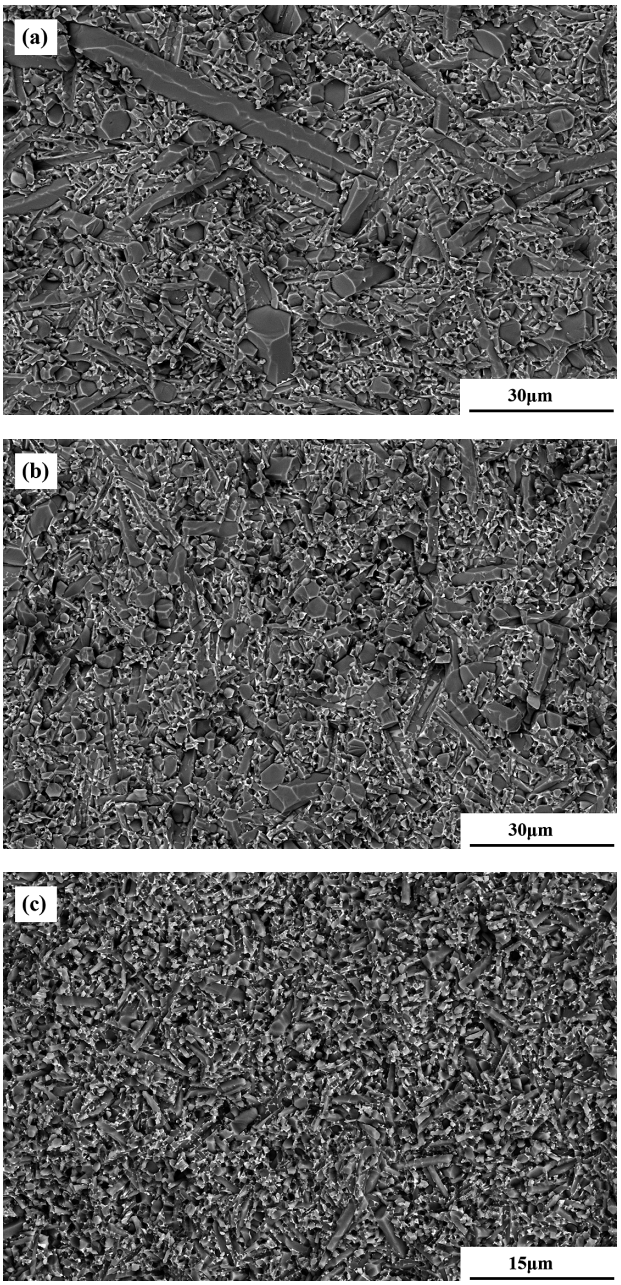

Fig. 16 SEM photographs of the fracture surfaces of Si_3N_4 samples prepared with different thermal conductivities: **(a)** Hitachi (120 W/(m·K)); **(b)** Maruwa (85 W/(m·K)); **(c)** PL sample. (Original work by the authors.)

gradually generating a Si_3N_4 layer; 4) when the thickness of the generated Si_3N_4 layer gradually increases, the reaction rate gradually decreases, and the reaction rate is determined by the gas diffusion rate (Chang et al., 2000; Jennings, 1983).

The thermal conductivity of Si_3N_4 ceramics prepared by atmospheric pressure sintering at this stage is low and cannot meet the index requirements of products at this stage. Pressureless sintering remains a potential process route for the future development of high thermal conductivity Si_3N_4 ceramic substrates. First, the lower temperature of atmospheric pressure sintering can reduce energy consumption and can reduce the dependence on high-end sintering equipment and reduce preparation costs. In view of the problem of the low thermal conductivity of pressureless sintered Si_3N_4 ceramics, the improvement pathway can choose to adopt SRBSN technology, as well as select an oxygen-free sintering additive system, and the need to reduce the content of sintering additives. Meanwhile, the grain size of pressureless sintered Si_3N_4 ceramics tends to be small (in **Fig. 16(c)**), so the thermal conductivity can be improved by adding suitable high-purity β-Si_3N_4 as a grain seed.

In our group, high-performance Si_3N_4 ceramic was prepared first for TiO_2, Y_2O_3, and MgO as pressureless sintering additives. Si_3N_4 ceramic with a relative density of 99.6 % and a flexural strength of 785 ± 23.3 MPa could be obtained using 3 mol% TiO_2 and sintered at 1800 °C for 2 h (Duan et al., 2023). In the present study, TiO_2 was selected as a low-temperature sintering additive. According to the grain size of the sample sintered with TiO_2, there are three possible routes of grain growth on the surface during the annealing process. First, when the existed β-Si_3N_4 grains with the exposed *c*-direction on the surface can serve as grain seeds, they only grow along the original directions (slop or perpendicular to the surface). Moreover, the growth of *a*- and *b*-directions is limited because of the steric hindrance effect. Second, when the existing grains nucleus (radius of Si_3N_4 grains larger than critical radius) in or surrounded by the liquid phases, they preferentially orient to the *c*-axis and perpendicular to the surface of the annealed sample. Third, heterogeneous nucleation occurs as Ti atoms in the liquid phase during the heating treatment process. Thus, the nucleation energy decreases, the critical radius of the nucleus decreases, the nucleation ratio and nucleation number increase, and the grain size becomes finer. Therefore, to prepare high-performance Si_3N_4 ceramics by low-temperature sintering, sintering additives with low-temperature eutectic points with SiO_2 are selected, which can produce a sufficient liquid phase at low temperature to promote densification; at the same time, other components are added to regulate the microstructure of the Si_3N_4 ceramics.

Acknowledgments

This work was supported by the National Natural Science Foundation of China (No. 52102082) and sponsored by the Shanghai Sailing Program (21YF1454500), the State Key Laboratory of High Performance Ceramics and Superfine Microstructure of Shanghai Institute Ceramics, Chinese Academy of Sciences.

References

Abe O., Sintering of silicon nitride with alkaline-earth nitrides, Ceramics International, 16 (1990) 53–60. https://doi.org/10.1016/0272-8842(90)90063-L

Akimune Y., Munakata F., Matsuo K., Hirosaki N., Okamoto Y., Misono K., Raman spectroscopic analysis of structural defects in hot isostatically pressed silicon nitride, Journal of the Ceramic Society of Japan, 107 (1999) 339–342. https://doi.org/10.2109/JCERSJ.107.339

Becher P.F., Painter G.S., Shibata N., Waters S.B., Lin H.-T., Effects of rare-earth (RE) intergranular adsorption on the phase transformation, microstructure evolution, and mechanical properties in silicon nitride with RE_2O_3 + MgO additives: RE = La, Gd, and Lu, Journal of the American Ceramic Society, 91 (2008) 2328–2336. https://doi.org/10.1111/j.1551-2916.2008.02448.x

Becher P.F., Sun E.Y., Plucknett K.P., Alexander K.B., Kang E.-S., Hirao K., Brito M.E., Microstructural design of silicon nitride with improved fracture toughness: I, effects of grain shape and size, Journal of the American Ceramic Society, 81 (1998) 2821–2830. https://doi.org/10.1111/j.1151-2916.1998.tb02702.x

Chang F.-W., Liou T.-H., Tsai F.-M., The nitridation kinetics of silicon powder compacts, Thermochimica Acta, 354 (2000) 71–80. https://doi.org/10.1016/s0040-6031(00)00432-9

Chen H., Wang W., Yu X., Zuo K.-h., Xia Y., Yin J., Liang H., Yao D., Zeng Y.-P., The effect of annealing temperature on flexural strength, dielectric loss and thermal conductivity of Si_3N_4 ceramics, Journal of Alloys and Compounds, 813 (2020) 152203. https://doi.org/10.1016/j.jallcom.2019.152203

Duan Y., Liu N., Zhang J., Zhang H., Li X., Cost effective preparation of Si_3N_4 ceramics with improved thermal conductivity and mechanical properties, Journal of the European Ceramic Society, 40 (2020) 298–304. https://doi.org/10.1016/j.jeurceramsoc.2019.10.003

Duan Y., Zhang J., Li X., Bai H., Sajgalik P., Jiang D., High thermal conductivity silicon nitride ceramics prepared by pressureless sintering with ternary sintering additives, International Journal of Applied Ceramic Technology, 16 (2019) 1399–1406. https://doi.org/10.1111/ijac.13220

Duan Y., Zhang J., Li X., Huang M., Shi Y., Xie J., Jiang D., Rare earth oxides on properties of pressureless sintered Si_3N_4 ceramics, Journal of Inorganic Materials, 32 (2017) 1275–1279. https://doi.org/10.15541/jim20170056

Duan Y., Zhang J., Li X., Shi Y., Xie J., Jiang D., Low temperature pressureless sintering of silicon nitride ceramics for circuit substrates in powder electronic devices, Ceramics International, 44 (2018) 4375–4380. https://doi.org/10.1016/j.ceramint.2017.12.033

Duan Y., Zhang J., Zhou B., Li X., Wang Q., Liu N., Li Z., Wang L., Fabrication of high performance silicon nitride ceramics with TiO_2 additive by annealing process, Ceramics International, 49 (2023) 9035–9041. https://doi.org/10.1016/j.ceramint.2022.11.059

Feng T., Ruan X., Prediction of spectral phonon mean free path and thermal conductivity with applications to thermoelectrics and thermal management: A review, Journal of Nanomaterials, 2014 (2014) 206370. https://doi.org/10.1155/2014/206370

Fu S., Yang Z., Li H., Wang L., Li Y., Li J., Effects of Gd_2O_3 and $MgSiN_2$ sintering additives on the thermal conductivity and mechanical properties of Si_3N_4 ceramics, International Journal of Applied Ceramic Technology, 20 (2022) 1855–1864. https://doi.org/10.1111/ijac.14279

Golla B.R., Ko J.W., Kim J.-M., Kim H.-D., Effect of particle size and oxygen content of Si on processing, microstructure and thermal

conductivity of sintered reaction bonded Si_3N_4, Journal of Alloys and Compounds, 595 (2014) 60–66. https://doi.org/10.1016/j.jallcom.2014.01.131

Guo W.-M., Wu L.-X., Ma T., You Y., Lin H.-T., Rapid fabrication of Si_3N_4 ceramics by reaction-bonding and pressureless sintering, Journal of the European Ceramic Society, 36 (2016) 3919–3924. https://doi.org/10.1016/j.jeurceramsoc.2016.06.007

Gutiérrez C.A., Moreno R., Tape casting of non-aqueous silicon nitride slips, Journal of the European Ceramic Society, 20 (2000) 1527–1537. https://doi.org/10.1016/S0955-2219(99)00216-2

Haggerty J., Lightfoot A., Opportunities for enhancing the thermal conductivities of SiC and Si_3N_4 ceramics through improved processing, Ceramic Engineering & Science Proceedings, (1995) 475–487. https://doi.org/10.1002/9780470314715.ch52

Haggerty J.S., Lightfoot A., Ritter J.E., Gennari P.A., Nair S.V., Oxidation and fracture strength of high-purity reaction-bonded silicon nitride, Journal of the American Ceramic Society, 72 (1989) 1675–1679. https://doi.org/10.1111/j.1151-2916.1989.tb06302.x

Hayashi H., Hirao K., Kitayama M., Yamauchi Y., Kanzaki S., Effect of oxygen content on thermal conductivity of sintered silicon nitride, Journal of the Ceramic Society of Japan, 109 (2001a) 1046–1050. https://doi.org/10.2109/jcersj.109.1276_1046

Hayashi H., Hirao K., Toriyama M., Kanzaki S., Itatani K., $MgSiN_2$ addition as a means of increasing the thermal conductivity of β-silicon nitride, Journal of the American Ceramic Society, 84 (2001b) 3060–3062. https://doi.org/10.1111/j.1151-2916.2001.tb01141.x

Hirao K., Watari K., Brito M.E., Toriyama M., Kanzaki S., High thermal conductivity in silicon nitride with anisotropic microstructure, Journal of the American Ceramic Society, 79 (1996) 2485–2488. https://doi.org/10.1111/j.1151-2916.1996.tb09002.x

Hirao K., Watari K., Hayashi H., Kitayama M., High thermal conductivity silicon nitride ceramic, MRS Bulletin - Materials Research Society, 26 (2001) 451–457. https://doi.org/10.1557/mrs2001.115

Hirao K., Zhou Y., Miyazaki H., Hyuga H., Improvement in thermal conductivity of silicon nitride ceramics via microstructural control and their application to heat dissipation substrates, Journal of the Japan Society of Powder and Powder Metallurgy, 64 (2017) 439–444. https://doi.org/10.2497/jjspm.64.439

Hirosaki N., Ogata S., Kocer C., Kitagawa H., Nakamura Y., Molecular dynamics calculation of the ideal thermal conductivity of single-crystal α- and β-Si_3N_4, Physical Review B, 65 (2002) 134110. https://doi.org/10.1103/PhysRevB.65.134110

Hirosaki N., Okamoto Y., Ando M., Munakata F., Akimune Y., Thermal conductivity of gas-pressure-sintered silicon nitride, Journal of the American Ceramic Society, 79 (1996) 2878–2882. https://doi.org/10.1111/j.1151-2916.1996.tb08721.x

Hu F., Zhao L., Xie Z.P., Silicon nitride ceramics with high thermal conductivity and excellent mechanical properties fabricated with MgF_2 sintering aid and post-sintering heat treatment, Journal of Ceramic Science and Technology, 07 (2016) 423–428. https://doi.org/10.4416/JCST2016-00065

Hu F., Zhu T., Xie Z., Liu J., Effect of composite sintering additives containing non-oxide on mechanical, thermal and dielectric properties of silicon nitride ceramics substrate, Ceramics International, 47 (2021) 13635–13643. https://doi.org/10.1016/j.ceramint.2021.01.224

Huang M., Huang Y., Ou J., Wu Y., Wang J., Wu S., Effect of a new non-oxide additive, $Y_3Si_2C_2$, on the thermal conductivity and mechanical properties of Si_3N_4 ceramics, International Journal of Applied Ceramic Technology, 19 (2022) 3403–3409. https://doi.org/10.1111/ijac.14132

Imamura H., Hirao K., Brito M.E., Toriyama M., Kanzaki S., Further improvement in mechanical properties of highly anisotropic silicon nitride ceramics, Journal of the American Ceramic Society, 83 (2000) 495–500. https://doi.org/10.1111/j.1151-2916.2000.tb01223.x

Jennings H.M., Review on reactions between silicon and nitrogen: part 1 mechanisms, Journal of Materials Science, 18 (1983) 951–967. https://doi.org/10.1007/bf00551961

Jiang G.J., Xu J.Y., Peng G.H., Zhuang H.R., Li W.L., Xu S.Y., Mao Y.J., Sintering of silicon nitride ceramics with magnesium silicon nitride and yttrium oxide as sintering aids, Materials Science and Engineering, 18 (2011) 202017. https://doi.org/10.1088/1757-899X/18/20/202017

Kaidash O.N., Fesenko I.P., Kryl Y.A., Heat Conductivity, Physicomechanical properties and interrelations of them and structures of pressureless sintered composites produced of Si_3N_4–Al_2O_3–Y_2O_3(–ZrO_2) nanodispersed system, Journal of Superhard Materials, 36 (2014) 96–104. https://doi.org/10.3103/S106345761402004X

Kim J.-M., Ko S.-I., Kim H.-N., Ko J.-W., Lee J.-W., Kim H.-D., Park Y.-J., Effects of microstructure and intergranular glassy phases on thermal conductivity of silicon nitride, Ceramics International, 43 (2017) 5441–5449. https://doi.org/10.1016/j.ceramint.2017.01.037

Kingery W.D., Densification during sintering in the presence of a liquid phase: I. theory, Journal of Applied Physics, 30 (1959) 301–306. https://doi.org/10.1063/1.1735155

Kingery W.D., Narasimhan M.D., Densification during sintering in the presence of a liquid phase: II. experimental, Journal of Applied Physics, 30 (1959) 307–310. https://doi.org/10.1063/1.1735156

Kitayama M., Hirao K., Kanzaki S., Effect of rare earth oxide additives on the phase transformation rates of Si_3N_4, Journal of the American Ceramic Society, 89 (2006) 2612–2618. https://doi.org/10.1111/j.1551-2916.2006.01106.x

Kitayama M., Hirao K., Toriyama M., Kanzaki S., Modeling and simulation of grain growth in Si_3N_4: I. anisotropic Ostwald ripening, Acta Materialia, 46 (1998a) 6541–6550. https://doi.org/10.1016/S1359-6454(98)00290-0

Kitayama M., Hirao K., Toriyama M., Kanzaki S., Modeling and simulation of grain growth in Si_3N_4: II. the α–β transformation, Acta Materialia, 46 (1998b) 6551–6557. https://doi.org/10.1016/S1359-6454(98)00291-2

Kitayama M., Hirao K., Toriyama M., Kanzaki S., Control of β-Si_3N_4 crystal morphology and its mechanism (part 1), Journal of the Ceramic Society of Japan, 107 (1999a) 930–934. https://doi.org/10.2109/JCERSJ.107.930

Kitayama M., Hirao K., Toriyama M., Kanzaki S., Thermal conductivity of β-Si_3N_4: I, effects of various microstructural factors, Journal of the American Ceramic Society, 82 (1999b) 3105–3112. https://doi.org/10.1111/j.1151-2916.1999.tb02209.x

Kitayama M., Hirao K., Tsuge A., Watari K., Toriyama M., Kanzaki S., Thermal conductivity of β-Si_3N_4: II, effect of lattice oxygen, Journal of the American Ceramic Society, 83 (2000) 1985–1992. https://doi.org/10.1111/j.1151-2916.2000.tb01501.x

Kitayama M., Hirao K., Watari K., Toriyama M., Kanzaki S., Thermal conductivity of β-Si_3N_4: III, effect of rare-earth (RE = La, Nd, Gd, Y, Yb, and Sc) oxide additives, Journal of the American Ceramic Society, 84 (2001) 353–358 https://doi.org/10.1111/j.1151-2916.2001.tb00662.x

Kong J.H., Ma H.J., Jung W.K., Hong J., Jun K., Kim D.K., Self-reinforced and high-thermal conductivity silicon nitride by tailoring α-β phase ratio with pressureless multi-step sintering, Ceramics International, 47 (2021) 13057–13064. https://doi.org/10.1016/j.ceramint.2021.01.169

Krause Jr R.F., Wiederhorn S.M., Li C.-W., Tensile creep behavior of a gas-pressure-sintered silicon nitride containing silicon carbide, Journal of the American Ceramic Society, 84 (2001) 2394–2400. https://doi.org/10.1111/j.1151-2916.2001.tb01020.x

Kumar K., Park Y.-J., Kim M.-J., Kim H.-N., Jin Ma H., Lee J.-W., Ko J.-W., Influence of ternary oxide additives on thermal conductivity of pressureless sintered Si_3N_4, Materials Letters, 328 (2022) 133189. https://doi.org/10.1016/j.matlet.2022.133189

Kusano D., Hyuga H., Zhou Y., Hirao K., Effect of aluminum content on mechanical properties and thermal conductivities of sintered reaction-bonded silicon nitride, International Journal of Applied Ceramic Technology, 11 (2014) 534–542. https://doi.org/10.1111/ijac.12035

Kusano D., Noda Y., Shibasaki H., Hyuga H., Zhou Y., Hirao K., Effects of impurity iron content on characteristics of sintered reaction-bonded silicon nitride, International Journal of Applied Ceramic Technology, 10 (2013) 690–700. https://doi.org/10.1111/j.1744-7402.2012.02767.x

Lee H.M., Lee E.B., Kim D.L., Kim D.K., Comparative study of oxide

and non-oxide additives in high thermal conductive and high strength Si_3N_4 ceramics, Ceramics International, 42 (2016) 17466–17471. https://doi.org/10.1016/j.ceramint.2016.08.051

Lee S.-H., Densification, mass loss, and mechanical properties of low-temperature pressureless-sintered Si_3N_4 with $LiYO_2$ additive: the effects of additive content and annealing, International Journal of Applied Ceramic Technology, 7 (2010) 881–888. https://doi.org/10.1111/j.1744-7402.2009.02402.x

Lee S.-K., Yamada I., Kume S., Nakano H., Hatori K., Matsui G., Watari K., Thermal conductivity measurement at the micrometer scale of ceramics using thermoreflectance technique —High-thermal-conductivity AlN with reduced amount of grain boundary phase, Journal of the Ceramic Society of Japan, 116 (2008) 1260–1264. https://doi.org/10.2109/jcersj2.116.1260

Legut D., Wdowik U.D., Kurtyka P., Vibrational and dielectric properties of α-Si_3N_4 from density functional theory, Materials Chemistry and Physics, 147 (2014) 42–49. https://doi.org/10.1016/j.matchemphys.2014.03.058

Li B., Pottier L., Roger J.P., Fournier D., Watari K., Hirao K., Measuring the anisotropic thermal diffusivity of silicon nitride grains by thermoreflectance microscopy, Journal of the European Ceramic Society, 19 (1999) 1631–1639. https://doi.org/10.1016/S0955-2219(98)00258-1

Li J., Jiang Q., Pan Z., Lv D., Wu S., Fabrication of silicon nitride with high thermal conductivity and flexural strength by hot-pressing flowing sintering, International Journal of Applied Ceramic Technology, 21 (2024) 2841–2849. https://doi.org/10.1111/ijac.14741

Li Y., Kim H.-N., Wu H., Kim M.-J., Ko J.-W., Kim J.-M., Park Y.-J., Huang Z., Kim H.-D., Improved thermal conductivity of sintered reaction-bonded silicon nitride using a BN/graphite powder bed, Journal of the European Ceramic Society, 37 (2017) 4483–4490. https://doi.org/10.1016/j.jeurceramsoc.2017.05.045

Li Y., Kim H.-N., Wu H., Kim M.-J., Ko J.-W., Park Y.-J., Huang Z., Kim H.-D., Enhanced thermal conductivity in Si_3N_4 ceramic with the addition of $Y_2Si_4N_6C$, Journal of the American Ceramic Society, 101 (2018) 4128–4136. https://doi.org/10.1111/jace.15544

Li Y., Kim H.-N., Wu H., Kim M.-J., Ko J.-W., Park Y.-J., Huang Z., Kim H.-D., Enhanced thermal conductivity in Si_3N_4 ceramic by addition of a small amount of carbon, Journal of the European Ceramic Society, 39 (2019) 157–164. https://doi.org/10.1016/j.jeurceramsoc.2018.10.006

Li Y., Kim H.-N., Wu H., Kim M.-J., Ko J.-W., Park Y.-J., Huang Z., Kim H.-D., Microstructure and thermal conductivity of gas-pressure-sintered Si_3N_4 ceramic: the effects of Y_2O_3 additive content, Journal of the European Ceramic Society, 41 (2021) 274–283. https://doi.org/10.1016/j.jeurceramsoc.2020.08.035

Liang H., Zeng Y., Zuo K., Xia Y., Yao D., Yin J., Mechanical properties and thermal conductivity of Si_3N_4 ceramics with YF_3 and MgO as sintering additives, Ceramics International, 42 (2016) 15679–15686. https://doi.org/10.1016/j.ceramint.2016.07.024

Liao S., Zhou L., Jiang C., Wang J., Zhuang Y., Li S., Thermal conductivity and mechanical properties of Si_3N_4 ceramics with binary fluoride sintering additives, Journal of the European Ceramic Society, 41 (2021) 6971–6982. https://doi.org/10.1016/j.jeurceramsoc.2021.07.035

Liu Y., Liu R., Zheng Y., Zhao J., Sui T., Li X., Lin B., Effect of the ratio of Y_2O_3 and $MgSiN_2$ sintering additives on the microstructure, thermal and mechanical properties of Si_3N_4 ceramics, Ceramics International, 49 (2023) 36490–36496. https://doi.org/10.1016/j.ceramint.2023.08.332

Lu T., Wang T., Jia Y., Ding M., Shi Y., Xie J., Lei F., Zhang L., Fan L., Fabrication of high thermal conductivity silicon nitride ceramics by pressureless sintering with MgO and Y_2O_3 as sintering additives, Ceramics International, 46 (2020) 27175–27183. https://doi.org/10.1016/j.ceramint.2020.07.198

Luo C., Zhang Y., Deng T., Pressureless sintering of high performance silicon nitride ceramics at 1620 °C, Ceramics International, 47 (2021) 29371–29378. https://doi.org/10.1016/j.ceramint.2021.07.104

Matovic B., Boskovic S., Thermal conductivity of pressureless sintered Si_3N_4 ceramics with Li-exchanged zeolite, Journal of the Serbian Chemical Society, 69 (2004) 705–710. https://doi.org/10.2298/JSC0409705M

Matovic B., Rixecker G., Golczewski J., Aldinger F., Thermal conductivity of pressureless sintered silicon nitride materials with $LiYO_2$ additive, Science of Sintering, 36 (2004) 3–9. https://doi.org/10.2298/SOS0401003M

Moulson A.J., Review, reaction-bonded silicon nitride its formation and properties, Journal of Materials Science, 14 (1979) 1017–1051. https://doi.org/10.1007/bf00561287

Niihara K., Hirai T., Chemical vapour-deposited silicon nitride, Journal of Materials Science, 12 (1977) 1243–1252. https://doi.org/10.1007/BF00553616

Ogata S., Hirosaki N., Kocer C., Shibutani Y., A comparative ab initio study of the 'ideal' strength of single crystal α- and β-Si_3N_4, Acta Materialia, 52 (2004) 233–238. https://doi.org/10.1016/j.actamat.2003.09.008

Ohashi M., Nakamura K., Hirao K., Kanzaki S., Hampshire S., Formation and properties of Ln-Si-O-N glasses (Ln = Lanthanides or Y), Journal of the American Ceramic Society, 78 (1995) 71–76. https://doi.org/10.1111/j.1151-2916.1995.tb08362.x

Okumura H., Present status and future prospect of widegap semiconductor high-power devices, Japanese Journal of Applied Physics, 45 (2006) 7565. https://doi.org/10.1143/jjap.45.7565

Park C., Bang K.-S., Park D.-S., Kim H.-D., Danyluk S., Pressureless-sintering of reaction bonded silicon nitride containing cordierite, Journal of Ceramic Processing Research, 13 (2012) 226–230.

Riley F.L., Silicon nitride and related materials, Journal of the American Ceramic Society, 83 (2000) 245–265. https://doi.org/10.1111/j.1151-2916.2000.tb01182.x

Sakka Y., Fabrication of ceramics with highly controlled microstructures by advanced fine powder processing, KONA Powder and Particle Journal, 36 (2019) 114–128. https://doi.org/10.14356/kona.2019007

Shibata N., Pennycook S.J., Gosnell T.R., Painter G.S., Shelton W.A., Becher P.F., Observation of rare-earth segregation in silicon nitride ceramics at subnanometre dimensions, Nature, 428 (2004) 726–730. https://doi.org/10.1038/nature02445

Suematsu H., Mitomo M., Mitchell T.E., Petrovic J.J., Fukunaga O., Ohashi N., The α–β Transformation in Silicon Nitride Single Crystals, Journal of the American Ceramic Society, 80 (2005) 615–620. https://doi.org/10.1111/j.1151-2916.1997.tb02876.x

Sun E.Y., Becher P.F., Plucknett K.P., Hsueh C.-H., Alexander K.B., Waters S.B., Hirao K., Brito M.E., Microstructural design of silicon nitride with improved fracture toughness: II, Effects of yttria and alumina additives, Journal of the American Ceramic Society, 81 (1998) 2831–2840. https://doi.org/10.1111/j.1151-2916.1998.tb02703.x

Tanaka K., Zaki K., Martin C., Sintering of Si_3N_4-HIP map for liquid phase sintering, Proceedings of the International Conference on Hot Isostatic Pressing, Sweden, Centiek, (1987).

Tiwari J., Feng T., Accurate prediction of thermal conductivity of Al_2O_3 at ultrahigh temperatures, Physical Review B, 109 (2024) 075201. https://doi.org/10.1103/PhysRevB.109.075201

Tsukuma K., Shimada M., Koizumi M., Thermal conductivity and microhardness of Si_3N_4 with and without additives, American Ceramic Society Bulletin, 60 (1981) 910–912.

Wang C.-M., Pan X., Rühle M., Riley F.L., Mitomo M., Silicon nitride crystal structure and observations of lattice defects, Journal of Materials Science, 31 (1996) 5281–5298. https://doi.org/10.1007/BF01159294

Wang L., Qi Q., Cai P., Zhang H., Yang X., Liu X., Jiao Z., Huang Z., New route to improve the fracture toughness and flexural strength of Si_3N_4 ceramics by adding $FeSi_2$, Scripta Materialia, 126 (2017) 11–14. https://doi.org/10.1016/j.scriptamat.2016.08.012

Wang W., Yao D., Chen H., Xia Y., Zuo K., Yin J., Liang H., Zeng Y.P., $ZrSi_2$–MgO as novel additives for high thermal conductivity of β-Si_3N_4 ceramics, Journal of the American Ceramic Society, 103 (2019) 2090–2100. https://doi.org/10.1111/jace.16902

Wang W., Yao D., Liang H., Xia Y., Zuo K., Yin J., Zeng Y.-P., Effect of in-situ formed Y_2O_3 by metal hydride reduction reaction on thermal

conductivity of β-Si_3N_4 ceramics, Journal of the European Ceramic Society, 40 (2020a) 5316–5323. https://doi.org/10.1016/j.jeurceramsoc.2020.06.005

Wang W., Yao D., Liang H., Xia Y., Zuo K., Yin J., Zeng Y.P., Effect of the binary nonoxide additives on the densification behavior and thermal conductivity of Si_3N_4 ceramics, Journal of the American Ceramic Society, 103 (2020b) 5891–5899. https://doi.org/10.1111/jace.17282

Wang W., Yao D., Liang H., Xia Y., Zuo K., Yin J., Zeng Y.-P., Enhanced thermal conductivity in Si_3N_4 ceramics prepared by using ZrH_2 as an oxygen getter, Journal of Alloys and Compounds, 855 (2021) 157451. https://doi.org/10.1016/j.jallcom.2020.157451

Wang Y., Jones S., Dai A., Liu G., Reliability enhancement by integrated liquid cooling in power IGBT modules for hybrid and electric vehicles, Microelectronics Reliability, 54 (2014a) 1911–1915. https://doi.org/10.1016/j.microrel.2014.07.037

Wang Z.H., Bai B., Ning X.S., Effect of rare earth additives on properties of silicon nitride ceramics, Advances in Applied Ceramics, 113 (2014b) 173–177. https://doi.org/10.1179/1743676113y.0000000138

Wasanapiaenpong T., Wada S., Imai M., Yano T., Lower temperature pressureless sintering of Si_3N_4 ceramics using SiO_2-MgO-Y_2O_3 additives without packing powder, Journal of the Ceramic Society of Japan, 114 (2006) 733–738. https://doi.org/10.2109/jcersj.114.733

Watari K., Evaluation of thermal conductivity of grains and fillers by using thermoreflectance technique—Si_3N_4, AlN, SiC, Journal of the Ceramic Society of Japan, 122 (2014) 967–970. https://doi.org/10.2109/jcersj2.122.967

Watari K., Hirao K., Brito M.E., Toriyama M., Kanzaki S., Hot isostatic pressing to increase thermal conductivity of Si_3N_4 ceramics, Journal of Materials Research, 14 (1999) 1538–1541. https://doi.org/10.1557/JMR.1999.0206

Watari K., Seki Y., Ishizaki K., Temperature dependence of thermal coefficients for HIPped silicon nitride, Journal of the Ceramic Society of Japan, 97 (1989) 174–181. https://doi.org/10.2109/jcersj.97.174

Yamada T., Preparation and evaluation of sinterable silicon nitride powder by imide decomposition method, American Ceramic Society Bulletin, 72 (1993) 99–106. https://www.osti.gov/biblio/6486823

Yang H., Yang G., Yuan R., Pressureless sintering of silicon nitride with magnesia and ceria, Materials Research Bulletin, 33 (1998) 1467–1473. https://doi.org/10.1016/S0025-5408(98)00129-9

Yokota H., Ibukiyama M., Effect of lattice impurities on the thermal conductivity of β Si_3N_4, Journal of the European Ceramic Society, 23 (2003) 55–60. https://doi.org/10.1016/S0955-2219(02)00074-2

Yoshida K., Sekimoto Y., Katayama K., Wasanapiarnpong T., Imai M., Yano T., The Effect of heat-treatment on thermal conductivity of silicon nitride ceramics, Key Engineering Materials, 484 (2011) 52–56. https://doi.org/10.4028/www.scientific.net/KEM.484.52

Zhang J., Cui W., Li F., Du S., Tian Z., Sun S., Chen K., Liu G., Effects of $MgSiN_2$ addition and post-annealing on mechanical and thermal properties of Si_3N_4 ceramics, Ceramics International, 46 (2020) 15719–15722. https://doi.org/10.1016/j.ceramint.2020.03.097

Zhang J., Ye F., Jiang D., Iwasa M., Preparation of bulk Si_3N_4 from tape casting and lamination, Ceramics International, 32 (2006) 277–282. https://doi.org/10.1016/j.ceramint.2005.03.003

Zhao J., Liu Y., Zheng Y., Li X., Sui T., Lin B., Fabrication of Si_3N_4 ceramics substrates with high thermal conductivity by tape casting and gas pressure sintering, International Journal of Applied Ceramic Technology, 21 (2024) 1493–1501. https://doi.org/10.1111/ijac.14694

Zhou Y., Hyuga H., Kusano D., Yoshizawa Y.-i., Hirao K., A tough silicon nitride ceramic with high thermal conductivity, Advanced Materials, 23 (2011) 4563–4567. https://doi.org/10.1002/adma.201102462

Zhou Y., Hyuga H., Kusano D., Yoshizawa Y., Ohji T., Hirao K., Development of high-thermal-conductivity silicon nitride ceramics, Journal of Asian Ceramic Societies, 3 (2015) 221–229. https://doi.org/10.1016/j.jascer.2015.03.003

Zhou Y., Zhu X., Hirao K., Lences Z., Sintered reaction-bonded silicon nitride with high thermal conductivity and high strength, International Journal of Applied Ceramic Technology, 5 (2008) 119–126. https://doi.org/10.1111/j.1744-7402.2008.02187.x

Zhu X., Sakka Y., Textured silicon nitride: processing and anisotropic properties, Science and Technology of Advanced Materials, 9 (2008) 033001. https://doi.org/10.1088/1468-6996/9/3/033001

Zhu X., Sakka Y., Suzuki T.S., Uchikoshi T., Kikkawa S., The c-axis texturing of seeded Si_3N_4 with β-Si_3N_4 whiskers by slip casting in a rotating magnetic field, Acta Materialia, 58 (2010a) 146–161. https://doi.org/10.1016/j.actamat.2009.08.064

Zhu X., Sakka Y., Zhou Y., Hirao K., The effect of embedding conditions on the thermal conductivity of β-Si_3N_4, Journal of the Ceramic Society of Japan, 114 (2006a) 1093–1096. https://doi.org/10.2109/JCERSJ.114.1093

Zhu X., Sakka Y., Zhou Y., Hirao K., Processing and properties of sintered reaction-bonded silicon nitride with Y_2O_3–$MgSiN_2$: effects of Si powder and Li_2O addition, Acta Materialia, 55 (2007a) 5581–5591. https://doi.org/10.1016/j.actamat.2007.06.014

Zhu X., Sakka Y., Zhou Y., Hirao K., Itatani K., A strategy for fabricating textured silicon nitride with enhanced thermal conductivity, Journal of the European Ceramic Society, 34 (2014) 2585–2589. https://doi.org/10.1016/j.jeurceramsoc.2014.01.025

Zhu X., Suzuki T.S., Uchikoshi T., Sakka Y., Texturing of Si_3N_4 ceramics via strong magnetic field alignment, Key Engineering Materials, 368–372 (2008) 871–874. https://doi.org/10.4028/www.scientific.net/KEM.368-372.871

Zhu X., Zhou Y., Hirao K., Ishigaki T., Sakka Y., Potential use of only Yb_2O_3 in producing dense Si_3N_4 ceramics with high thermal conductivity by gas pressure sintering, Science and Technology of Advanced Materials, 11 (2010b) 065001. https://doi.org/10.1088/1468-6996/11/6/065001

Zhu X., Zhou Y., Hirao K., Lenčéš Z., Processing and thermal conductivity of sintered reaction-bonded silicon nitride: I, effect of Si powder characteristics, Journal of the American Ceramic Society, 89 (2006b) 3331–3339. https://doi.org/10.1111/j.1551-2916.2006.01195.x

Zhu X., Zhou Y., Hirao K., Lenčéš Z., Processing and thermal conductivity of sintered reaction-bonded silicon nitride: (II) effects of magnesium compound and yttria additives, Journal of the American Ceramic Society, 90 (2007b) 1684–1692. https://doi.org/10.1111/j.1551-2916.2006.01462.x

Ziegler A., Idrobo J.C., Cinibulk M.K., Kisielowski C., Browning N.D., Ritchie R.O., Interface structure and atomic bonding characteristics in silicon nitride ceramics, Science, 306 (2004) 1768–1770. https://doi.org/10.1126/science.1104173

Ziegler A., Kisielowski C., Hoffmann M.J., Ritchie R.O., Atomic resolution transmission electron microscopy of the intergranular structure of a Y_2O_3-containing silicon nitride ceramic, Journal of the American Ceramic Society, 86 (2003) 1777–1785. https://doi.org/10.1111/j.1151-2916.2003.tb03554.x

Ziegler G., Hasselman D.P.H., Effect of phase composition and microstructure on the thermal diffusivity of silicon nitride, Journal of Materials Science, 16 (1981) 495–503. https://doi.org/10.1007/BF00738642

Authors' Short Biographies

Dr. Yusen Duan studied materials sciences at the university of Chinese Academy of Sciences and completed his Ph.D. thesis on "Fabrication and properties of silicon nitride ceramics with high thermal conductivity and high strength" under Prof. Dr. Jingxian Zhang. Later, he worked at the Shanghai Institute of Ceramics (Chinese Academy of Sciences) as a postdoctoral 2020–2022. His research focuses on the preparation of silicon nitride powder and high-performance silicon nitride ceramic molding and sintering.

Yanyu Ye studied materials sciences and engineering at the university of Chinese Academy of Sciences and his Master's thesis on "Preparation and properties of high-temperature co-fired silicon nitride ceramics" under Prof. Dr. Jingxian Zhang.

Dr. Ning Liu studied materials sciences at ShanghaiTech University and completed her Ph.D. thesis on "Research on Preparation and Properties of Colored Silicon Nitride" under Prof. Dr. Jingxian Zhang. She later worked at the Wuzhen Laboratory as a postdoctoral since 2023. She is mainly engaged in the preparation of high-performance silicon nitride ceramics and the research and development of new composite materials.

Wenyu Tang studied English major at the University of International Relations. Later, he worked at the Shanghai Institute of Ceramics (Chinese Academy of Sciences) since 2018. He was mainly engaged in the molding, sintering, microstructure, mechanical, and thermal properties of advanced ceramic materials such as aluminum nitride, silicon nitride, and boron carbide and other pre-research work.

Hu Ruan studied heating engineering at the East China University of Science and Technology and completed his master thesis on "Study on Powder Flow Control Characteristics of Dense Phase Pneumatic Conveying and Pneumatic Logistics Transmission System" under Prof. Dr. Haifeng Lu. Later, he worked at the Shanghai Institute of Ceramics (Chinese Academy of Sciences) since 2023. Currently, he is mainly engaged in the synthesis of ceramic powders and the preparation of super-hard ceramics.

Prof. Jingxian Zhang studied materials sciences at the university of Chinese Academy of Sciences and completed his Ph.D. thesis on "Aqueous tape casting process and laminated non-oxide composites" under Prof. Dongliang Jiang. Jingxian Zhang was awarded the Shanghai Pujiang Talent Program in 2007. He developed the first high-thermal-conductivity silicon nitride ceramic system based on domestic raw materials. The study independently proposed the integration of preparation technology with completely independent intellectual property rights, and the key technical indexes were benchmarked against the product data of Toshiba, Japan. He currently serves as a member of the Ceramics Committee of the China Rare Earth Society and in other posts.